Kinematic modelling of the Mozambique rifted margin and associated thermal histories

N. Etheve, L. Jeanniot, T. Cornu, Jean-Paul Callot

KINEMATIC MODELLING OF THERMAL HISTORY OF THE MOZAMBIQUE RIFTED MARGIN

N. ETHEVE[a,b], L. JEANNIOT[c], T. CORNU[b], J.P. CALLOT[a]

[a] Université de Pau et des Pays de l'Adour, E2S UPPA, CNRS, Total, LFCR-IPRA, Avenue de l'Université, 64000 Pau, France

[b] Total SA, CSTJF, avenue Larribau, 64000 Pau, France

[c] Faculty of Geosciences, Mantle Dynamics and Theoretical geophysics, Utrecht University, Princetonlaan 8a, 3584 CB, Utrecht, The Netherlands

ABSTRACT

The thermal evolution and crustal nature along the Mozambique rifted margin is investigated using a forward kinematic modelling approach. The numerous plate reconstructions for the breakup of East Gondwana question the crustal nature of the Mozambique margin, especially in the vicinity of the Beira High and the Zambezi depression. Given the few geological and geophysical data available, it is necessary to propose simple but relevant hypotheses to calibrate the margin structure and evolution. Different scenarios were tested to examine the nature of the crust in the Beira High and the Zambezi depression (i.e. continental, oceanic, and mixed). As the margin thermal evolution is related to the crustal architecture and nature, we compared thermal modeling results to well data. Based on these observations, we favor a continental nature for the Beira High and the Zambezi depression. Given the widespread magmatism in the area and the possible variation of volcanic addition along-strike, we consider the presence of underplating in the Zambezi depression.

1. INRODUCTION

The separation of East Gondwana (Madagascar, Antarctica, Sri Lanka, India, Australia and New Zealand) from West Gondwana (Africa and South America) began in the Early to Middle Jurassic and resulted in the formation of several oceanic basins, including the South Atlantic and Indian oceans. The Somalia and Mozambique basins separated Africa from Madagascar and Antarctica in the Late Jurassic (Norton and Sclater, 1979; Le Pichon and Heirtzler, 1968; McElhinny, 1970). Although the relative motions between Africa and Antarctica during the rifting are well constrained, their initial configuration, the crustal fabric of the rifted margins and the position of the continent-ocean transition (COT) are not well known. Given these uncertainties, it is not surprising that several plate reconstruction models of Africa and Antarctica have been proposed (Cox, 1992; Eagles and König, 2008; König and Jokat, 2010; Leinweber and Jokat, 2012; Gaina et al., 2013, 2015; Davis et al., 2016; Nguyen et al., 2016; Reeves et al., 2016; Mueller et al., 2016, 2017; Thompson, 2017). Considering the great number of reconstruction models, it is important to evaluate several models for margin structures and thermal evolution.

In this study, we use kinematic models to propose a scenario of deformation and thermal evolution of the lithosphere during the development of the Mozambique passive margin. We use the code FEmargin (Jeanniot et al., 2016) to advect material and temperature through a sequence of lithosphere deformation events and to obtain a wide range of rift geometries. The model predicts crustal thinning leading to crustal breakup, sediment deposition, decompression melting with its extraction at the surface or underplated and local depth-dependent thinning. These features make FEmargin an ideal tool for quantitative calibration of the crustal architecture, and for generating a thermal history of rifted margins.

We focus this study on the Central Mozambique passive margin. We first review the geological setting and data, and explain the controversies and hypotheses for the history of the Mozambique rifted margin. Then, along with a description of the kinematic modelling tool we use, we list the geological and geophysical data required to perform the calibration. FEmargin modeling involves defining a series of

deformation events calibrated to match the present-day crustal architecture, and compatible with the rifting events of the Mozambique margin. We modelled 5 evolution history scenarios which differ by the crustal nature of the Zambezi depression and the Beira High : (1a) the Beira high and the Zambezi depression are underlain by continental crust with no magmatic underplating (Senkans et al., 2019); (1b) the Beira High and the Zambezi depression consist of continental crust with magmatic underplating in the Zambezi depression (Mueller et al., 2016, 2017); (1c) the Beira High and Zambezi depression both consist of continental crust characterized by a magmatic underplating; (2) the Beira High consists of continental crust and the Zambezi depression has an oceanic nature (Leinweber and Jokat, 2012); (3) the Beira High and the Zambezi depression have an oceanic origin (Reeves et al., 2016; Nguyen et al., 2016). In addition, for each scenario we perform several sensitivity tests of key parameters, which may control the thermal history, and crustal geometry of the margin to examine their relative contribution. Finally, we discuss the possible crustal nature of the Beira High and the Zambezi depression.

2. EASTERN AFRICAN GEOLOGICAL AND TECTONIC SETTING

The Mozambique volcanic margin is bounded by the Davie Fracture Zone and the Madagascar ridge in the east, and by the Mozambique ridge in the west (Fig. 1). This margin and the associated basin resulted from the breakup of South Gondwana and are often linked to the Karoo-Ferrar Large Igneous Province (LIP) event around 180 Ma (Duncan et al., 1997; Cox, 1992; Jourdan et al., 2008). The conjugate margin is located in the Riiser Larsen Sea in Antarctica. Because no public data on its crustal structure exists, we have not included this conjugate margin in our modelling. The modelling is performed on the refraction profile 20140010 of the MOCOM-cruise (Jokat, 2014; Mueller et al., 2016; 2017) which crosses the Beira High. The Beira High is a prominent high at the boundary of the Zambezi depression in the southwestern part of the margin (Fig. 1) (Mahanjane, 2012; Leinweber et al., 2012; Mueller et al., 2016; Senkans et al., 2019) (Fig. 1).

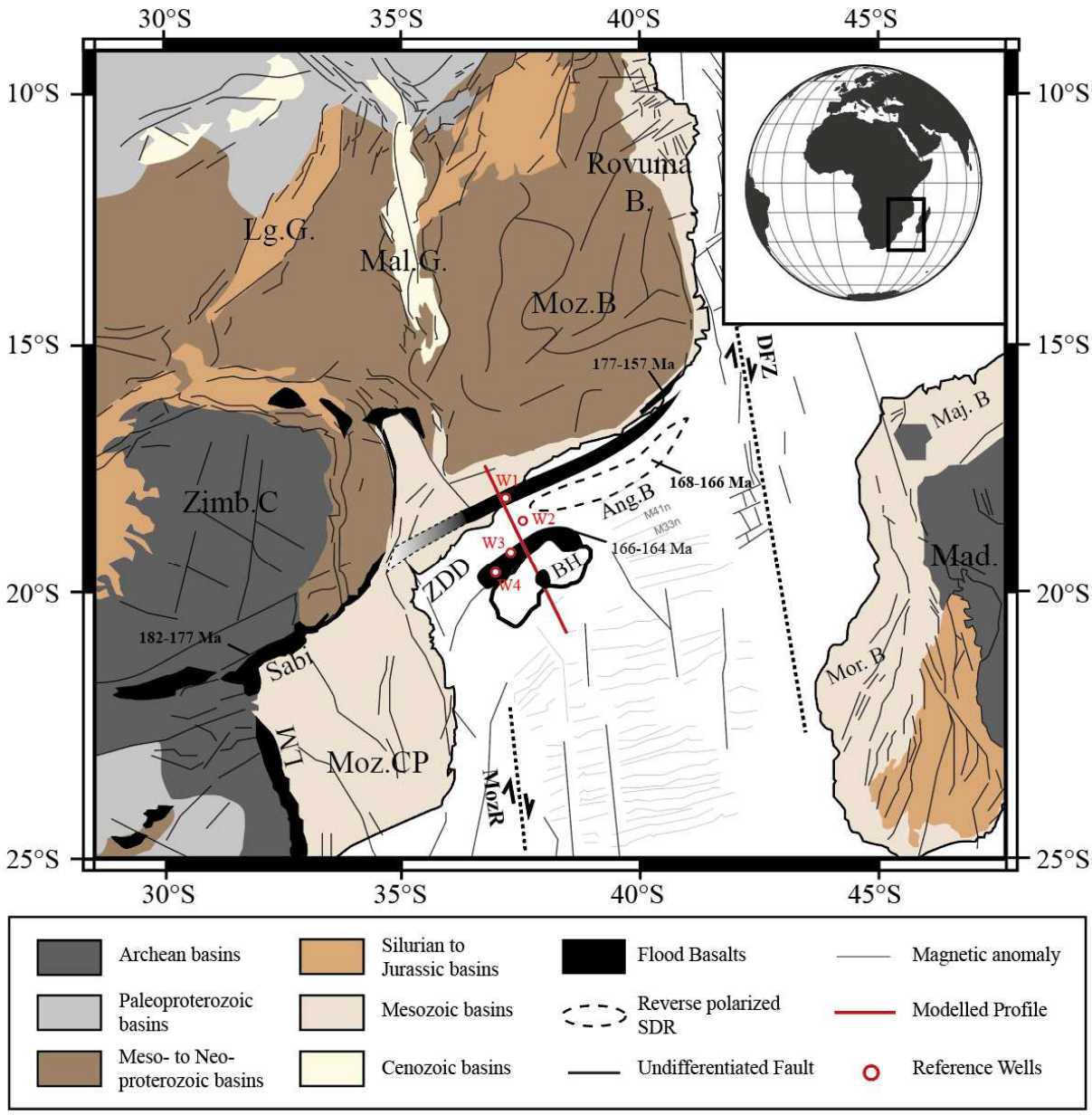

***Figure 1**: Geological and tectonic setting of the Mozambique Channel (modified after Mueller et al., 2016, 2017; Milesi et al., 2011). Approximate well locations for this study (Well 1 to Well 4) are shown as well as the modelled refraction profile of the MOCOM-Cruise (solid red line). The interpretation of the magnetic anomaly is from Leinweber et al. (2012) and Mueller and Jokat (2017). Abbreviations: Ang. B : Angoche Basin; BH : Beira High; DFZ : Davie Fracture Zone; Lg. B. : Lungwa Graben; LM : Lebombo Monocline; Mad. : Madagascar; Maj. B. : Majunga Basin; Mal. G. : Malawi Graben; Mor. B. :*

Morundava Basin; Moz. B. : Mozambique Basin; Moz. CP : Mozambique Coastal Plain; Rovuma B. : Rovuma Basin; Sabi : Mateke-Sabi Monocline; SDR : Seaward Dipping Reflectors ; ZDD : Zambezi Depression.

2.1. Timing of early rifting

The East African continental margin underwent several orogenic episodes from Paleoproterozoic (~2.2-1.8 Ga) to Neoproterozoic (~570-470 Ma) (Jacobs et al., 2003, 2008; Riedel et al., 2013), which are responsible for the formation of the Mozambican belt (Jacobs *et al.,* 2008; Bingen *et al.,* 2009). Following this collisional period, an extensional period corresponding to the Karoo rifting affected the Mozambique belt, from Carboniferous (~300 Ma) to Late Triassic (~200 Ma). The extensional deformation followed regional N-S, NW-SE and NE-SW trends, inherited from the underlying Proterozoic belt (Catuneanu et al., 2005). The Karoo rifting led to the deposition of Upper Carboniferous to Lower Jurassic sediments in large intracratonic basins across the Gondwana supercontinent. Some of these basins are covered by continental flood basalts in South Africa and Mozambique (Karoo igneous province), and in the Ferrar Province onshore East Antarctica (Riley et al., 2003; Thompson, 2017; Ponte, 2018) (Fig. 2).

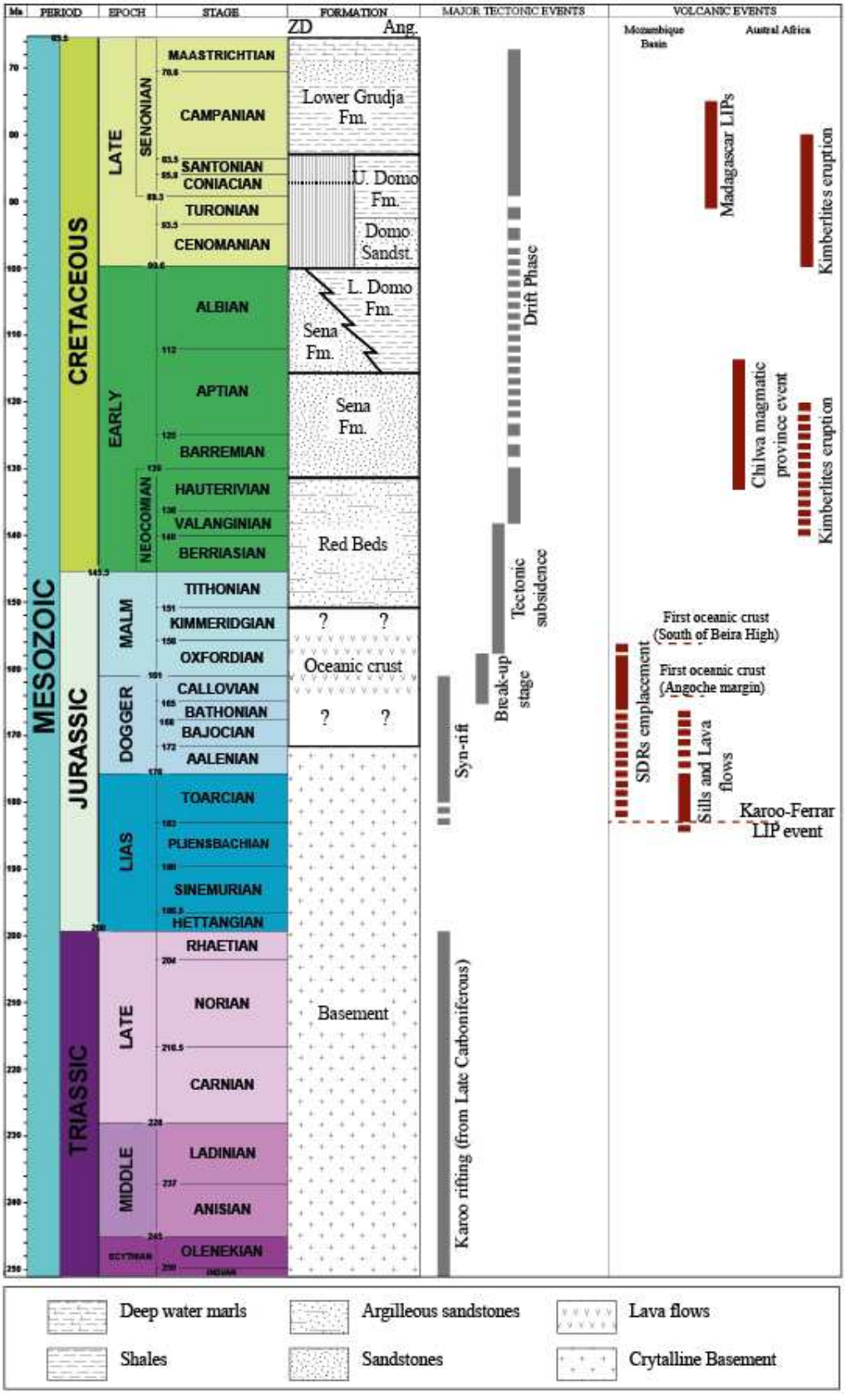
Ma
PERIOD
EPOCH
STAGE
FORMATION
ZD
Ang.
MAJOR TECTONIC EVENTS
VOLCANIC EVENTS
Mozambique Basin
Austral Africa
MESOZOIC
CRETACEOUS
JURASSIC
TRIASSIC
LATE
EARLY
MIDDLE
SENONIAN
NEOCOMIAN
MALM
DOGGER
LIAS
MAASTRICHTIAN
CAMPANIAN
SANTONIAN
CONIACIAN
TURONIAN
CENOMANIAN
ALBIAN
APTIAN
BARREMIAN
HAUTERIVIAN
VALANGINIAN
BERRIASIAN
TITHONIAN
KIMMERIDGIAN
OXFORDIAN
CALLOVIAN
BATHONIAN
BAJOCIAN
AALENIAN
TOARCIAN
PLIENSBACHIAN
SINEMURIAN
HETTANGIAN
RHAETIAN
NORIAN
CARNIAN
LADINIAN
ANISIAN
OLENEKIAN
Lower Grudja Fm.
U. Domo Fm.
Domo Sandst.
L. Domo Fm.
Sena Fm.
Sena Fm.
Red Beds
Oceanic crust
Basement
Karoo rifting (from Late Carboniferous)
Syn-rift
Break-up stage
Tectonic subsidence
Drift Phase
Madagascar LIPs
Kimberlites eruption
Chilwa magmatic province event
Kimberlites eruption
First oceanic crust (South of Beira High)
First oceanic crust (Angoche margin)
SDRs emplacement
Sills and Lava flows
Karoo-Ferrar LIP event
Deep water marls
Shales
Argilleous sandstones
Sandstones
Lava flows
Crytalline Basement

Figure 2: *Simplified tectonostratigraphic chart of the study area showing the major tectonic and volcanic events and the stratigraphy of the Zambezi delta depression (modified after Ponte, 2018; Mueller et al., 2017; Mahanjane et al., 2014). The geological time scale is from Gradstein et al. (2012).*

2.2. Cause of volcanism

The cause of the Karoo-Ferrar volcanism is still debated. A popular hypothesis involves a mantle plume origin (Burke and Dewey, 1973; Cox, 1992; Duncan et al., 1997); other studies have proposed upwelling of fertile asthenosphere or a lower continental mantle source (Bristow, 1983; Klausen, 2009; Hastie et al., 2016). The age of this igneous event is also debated. The following studies are mainly based on Ar-Ar and U-Pb zircon ages. The major peak of activity is dated to 200 – 190 Ma by Fitch and Miller (1984), or more recent at 183 ± 1 Ma by Duncan et al (1997). Recently, the Karoo basalts and sills of the southern African margin have been dated between 183.8 ± 2.4 and 176.2 ± 1.3 Ma (Segev, 2002; Jourdan et al., 2008; Svensen et al., 2012). Onshore along the southeastern African margin, the Lebombo and Mateke-Sabi monoclines form remnants of this volcanic province, emplaced around 190 Ma (Cox, 1992; Garner, 1996; Reeves, 2000; Watkeys, 2002; König and Jokat, 2006) or between 184 and 179 Ma (Duncan et al., 1997; Jourdan et al., 2005; Segev, 2002). A similar age of about 183 Ma for the igneous event was measured in the Ferrar flood basalts along the eastern Antarctica margin (Duncan et al., 1997; Encarnación et al., 1996).

Even though the Karoo event may not be directly involved in the breakup of Gondwana due to the time lag between these two events, it is possible that the large amount of volcanism played a role in the rifting through thermal weakening of the lithosphere (Storey et al., 1995), or by the development of major fault systems which helped to the localization of the deformation during extension (Thompson, 2017). In this study, we consider the initial stage of the Gondwana rifting to be characterized by the emplacement of the Karoo basalts on both conjugate margins at the same time, i.e. at roughly 183 ± 1 Ma (Fig. 2) (Duncan et al., 1997; Segev, 2002).

2.3. Plate motion

A wide range of hypotheses exist on the initial configuration of Gondwana and first movements between Africa and Antarctica (Smith and Hallem, 1970; König and Jokat, 2006; Eagles and König, 2008; Torsvik *et al.*, 2008; Leinweber *et al.*, 2012; Seton *et al.*, 2012; Gaina *et al.*, 2015, 2013; Reeves *et al.*, 2002, 2016). Indeed, the uncertainties about the magnetic anomalies in the Jurassic and Early Cretaceous periods (in particular the Jurassic Quiet Zone) (Leinweber and Jokat, 2012) question this initial plate configuration prior to rifting. In modern plate reconstructions, at least two stages of deformation are considered for the opening of the Mozambique Channel, with contrasted motions. During the first stage of deformation, it is suggested that Antarctica underwent either an anticlockwise rotation (Leinweber and Jokat, 2012), a strike-slip movement along an inherited shear zone (Senkans et al., 2019) or an E-W translation with respect to Africa (Cox, 1992). This first stage is proposed to have occurred between 190 Ma and 182 Ma, along with the Karoo-Ferrar igneous event (Duncan et al., 1997; Martin, 2007; Jourdan et al., 2007). During the second stage of deformation, Antarctica drifted southward along the Davie and Mozambique ridges. The age of this second event remains under discussion and may have begun around 170 Ma (Mahanjane, 2012), after 159 Ma (Leinweber et al., 2012), or later, around 153 Ma (Reeves et al., 2016) to 150 Ma (Phethean et al., 2016). Several authors assume the Zambezi depression located south of the Zambezi basin (Fig. 1) to be an aborted rift developed during this rifting stage, the activity of which ceased around 160 Ma due to a rift jump south of the Beira High (Senkans et al., 2019; Leinweber et al., 2012).

2.4. Oceanic domain

Identifying and interpreting marine magnetic anomalies is key to determine the age of the first oceanic crust between Antarctica and Africa. In the Riiser Larsen Sea offshore Antarctica, the oldest identified magnetic anomaly is M25 (~ 157 Ma) (Leitchenkov et al., 2008; König and Jokat, 2010; Leinweber and Jokat, 2012). In the Mozambican volcanic margin, previous studies identified M2 to M22 (~148 – 127 Ma) as the oldest magnetic anomalies (Segoufin, 1978; Simpson et al., 1979). Based on data obtained from a magnetic anomaly survey in 2005 and following the interpretation of Jokat et al. (2003),

König and Jokat (2010) proposed an age of M26n for the earliest oceanic crust (mid Kimmeridgian ca. 155 Ma). However, more recent studies proposed the anomalies M33n (Leinweber et al., 2012), or M41n (Leinweber and Jokat, 2013; Gaina et al., 2013) as the oldest anomalies in the Mozambique Basin (Early Oxfordian to Late Bathonian, respectively). Recent studies proposed that the rift jump and the first oceanic crust emplacement to be dated at 157± 3 Ma in the SE of the Beira High (Fig. 2) (Mueller et al. 2017; Senkans et al. 2018).

2.5. Crustal nature of the margin

An accurate determination of the crustal nature on both conjugate margins is critical to better constrain the rift evolution prior to the breakup. The nature of the crust of the Beira High and the offshore Zambezi depression is in the focus of this study (Fig. 4). Many plate reconstruction models propose an overlap of Antarctica on Africa at the present location of Beira High (Jokat et al., 2003; Seton et al., 2012; Torsvik et al., 2012; Leinweber and Jokat, 2012; Gaina et al., 2013; Reeves et al., 2016; Nguyen et al., 2016), assuming an oceanic origin for the Beira High such as a thickened oceanic crust or a magmatic structure (Watts, 2001; Mueller et al., 2016).

Other studies proposed a continental nature for the Beira High based on seismic reflection data (Mahanjane, 2012; Senkans et al., 2019). In particular, Mueller et al. (2016, 2017) present seismic refraction and gravity data supporting a continental origin for the Beira High and a possible intruded continental crust with a magmatic underplate, or a proto-oceanic crust within the offshore Zambezi depression (Mueller et al., 2017).

The nature of the crust within the Zambezi depression is also debated. The presence of continental crust would imply an aborted rift and a southward migration of the spreading ridge, leading to a breakup after 160 Ma south of Beira High (Mahanjane, 2012; Mueller et al., 2017; Senkans et al., 2018). Thus, the Beira High could be a more or less intruded microcontinent detached either from Africa or from Antarctica (Norton and Sclater, 1979; Martin and Hartnadu, 1986; Kovacs et al., 2002). Microcontinents

have been described in various geological context (rifting, strike-slip and subduction processes) and can result from several mechanisms of formation (Abera et al., 2016; Gaina et al., 2003; Torvisk et al., 2013; Van den Broek et al., 2019; Van den Broek and Gaina, 2020). In a rifted margin context, several possible factors can lead to microcontinents formation: a mantle plume interaction with continental lithosphere (Müller et al., 2002; Gaina et al., 2003; Torsvik et al., 2013), a magma-starved spreading ridge that is abandoned (Abera et al., 2016) or pre-existing lithospheric heterogeneities (Glerum et al., 2020).

An older breakup age is assumed if considering an oceanic crust within the Zambezi depression and/or the Beira High; in this case, the rift jump hypothesis is discarded and the margin presents the same evolution as observed in the Angoche margin where a breakup around 164 Ma (M38n.2n) is proposed by Mueller and Jokat (2017) (Fig. 2). The hypothesis of a crustal origin needs to be tested because pre-rift settings require a good knowledge of the crustal nature and therefore the location of the continent–ocean boundaries. Therefore, in this study we choose to model several scenarios based on the possible crustal nature and location of the COT along the Beira High profile.

3. NUMERICAL MODELLING METHODOLOGY

The evolution of the Mozambique volcanic margin from continental rifting to seafloor spreading is modelled using the kinematic code FEmargin (Jeanniot et al., 2016). The primary objective of the modelling is to calibrate and quantitatively constrain both the lithosphere and asthenosphere deformation at margin scale against geophysical and geological observations. After an overview of the model setup, we describe the data needed for the calibration and model parameterization. We will then present the modelled scenarios proposed for the Mozambique rifted margin.

3.1 Description of FEmargin

FEmargin is a kinematic numerical code that computes advection of lithosphere and asthenosphere temperature and material during continental rifting and breakup. This is achieved by setting multiple successive or simultaneous deformation events of finite duration. The deformation of lithosphere and

asthenosphere is prescribed by flow velocity fields, which are pre-generated in a finite element model using a layered Newtonian viscosity profile (Jeanniot et al., 2016). The pure shear flow fields are the main deformation modes, which result in passive upwelling beneath a deformation area (W), while the flow field buoyancy induced upwelling adds an active lithosphere thinning to pure shear. The location of the flow field axis may be controlled kinematically by migration or jump. Consequently, the migration of the pure-shear deformation axis acts like a simple shear mode (Wernicke, 1981) and thus produces an asymmetry in the margin architecture. Alternatively, the buoyancy induced upwelling acts like a local depth-dependent thinning.

We show in figure 3 the two flow fields, namely pure-shear + passive upwelling and buoyancy induced upwelling, separated 300 km apart from each other. Generic flow fields are pre-generated in a finite-element viscous flow model before they are used in FEmargin to advect lithosphere and asthenosphere material and temperature. Both flow fields are independently generated using the viscosity profile and the boundary conditions in red (V_x for the pure-shear flow field) and blue (V_z for the buoyancy induced upwelling) shown in figure 3. We varied the low viscosity layer width (W) to create several cases of pure-shear + passive upwelling deformation of varied width. Conversely, the viscosity profile used to generate the buoyancy-induced upwelling flow field is constrained to a certain depth range (i.e. buoyancy action depth in figure 3), above which no deformation from buoyancy upwelling is allowed. In both cases, we use a non-dimensional unit velocity so that we can simply multiply the flow-field unit magnitude with any given velocities in FEmargin.

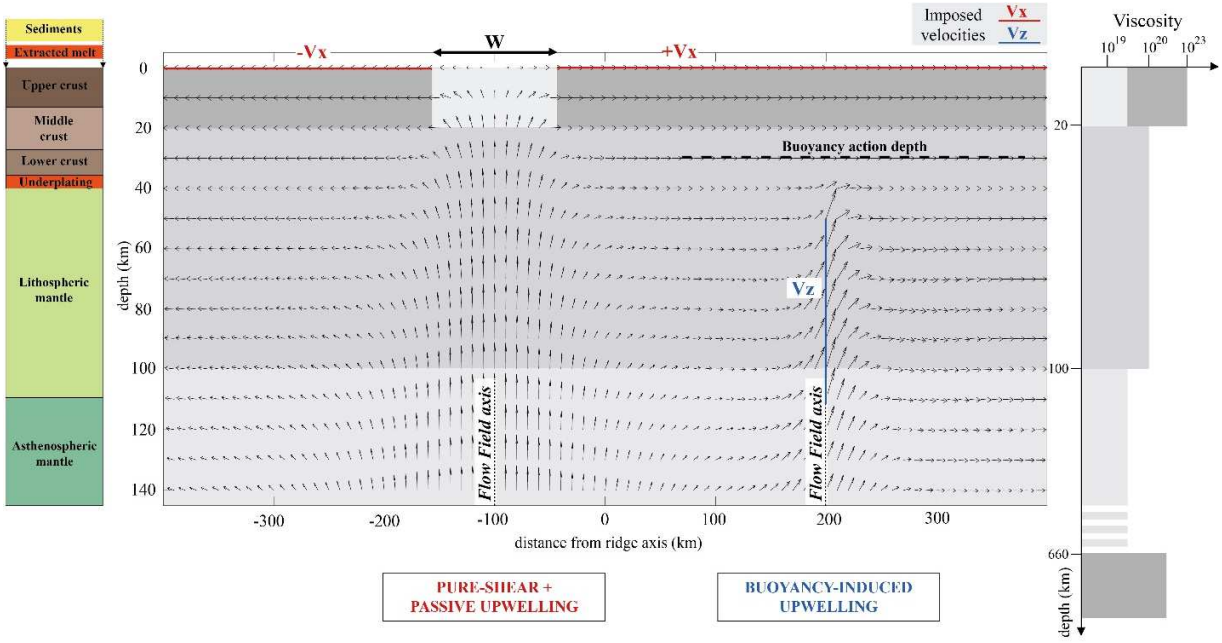

Figure 3: *Example of the two main deformation modes used in the kinematic approach. On the right is shown a profile of the Newtonian layered viscosity structure set in the 2D finite-element viscous flow model to create the flow fields. Red and blue solid lines are the boundary conditions of Vx and Vz, when generating the pure shear + passive upwelling and buoyancy induced upwelling deformation modes, respectively. The resulting two flow-fields have been added to each other in FEmargin as a single event. The flow fields are separated 300 km apart. The pure-shear flow field has a deformation half width of 50 km. The buoyancy induced upwelling is only active in the buoyancy window defined below 30 km depth. On the left is the color code used in FEmargin, which is unrelated to the viscosity profile. See text for more details.*

For the example shown in figure 3, the axis of the pure-shear flow field is located at -100 km, while the axis of the buoyancy flow-field is located at +200 km. The pure shear deformation half-width is set at 50 km, and the half-spreading rate at 10mm/yr. The magnitude of the buoyancy induced upwelling is also set at 10 mm/yr. Because both flow fields are simply added for each event set in FEmargin, we clearly see that the pure-shear flow field thus affects the upwelling flow-field, resulting in the buoyancy being

slightly deflected toward the right. The interference between the two flow-fields shows the importance of the control of the flow-field axis location by jumps or continuous migration, besides the production of an asymmetry of the margin. The continuous migration of a flow field axis is determined by a migration factor $F_m = V_m/V_x$, with V_m the axis migration velocity. Those flow fields are then used to advect material and temperature. For the temperature, we used the following advection-diffusion equation:

$$\frac{\partial T}{\partial t} = \frac{1}{\rho C_p}\nabla(k\nabla T) - \boldsymbol{V}(\nabla T + h) + \frac{A}{\rho C_p}$$

where T is the temperature, ρ the density, C_p the heat capacity, k the thermal conductivity, h the adiabatic gradient as described in McKenzie and Bickle (1988). A is the radiogenic heat productivity and $\mathbf{V}$ the applied velocity field.

Lithosphere and asthenosphere advection leads to crustal thinning, resulting in tectonic subsidence, thermal uplift and decompression melting. Decompression melting is parameterized following Katz et al. (2003) methodology for only dry peridotites. Once generated, the melt may be entirely or partially extracted to the surface or stored beneath the Moho as underplated material. There is no consensus about how much melt is extracted to the surface, retained in the mantle or underplated, and we rely on the calibration of the rifted margin, constrained with observation data, to estimate the percentage of melt required in each extraction process. The volume of melt, underplated or extracted to the surface, is then equally distributed along a certain width defined by the user. The extraction axis of melt at the surface or underplated may also continuously migrate laterally using a migration factor. In addition, two sediment deposition processes help to better constrain the crustal architecture of the studied margin: a global sedimentation rate for the entire profile, and an additional local coastal sedimentation rate to represent a continental sediment influx. Although there is no sediment compaction in FEmargin and the density of the sediments remains constant in time, FEmargin gives sufficient control on the deformation and thermal parameters to appropriately calibrate the studied margins.

The calibration procedure of the model against observations is as follows. The predicted model evolution of continental crustal thinning and lithosphere deformation is tracked with the top sediment, top volcanic, top basement, Moho, underplated melt level and the lithosphere-asthenosphere boundary interfaces. Those modelled interfaces should not only match the data, but the calibration also requires a good fit of the observed timing of extension, subsidence histories, melt and thermal data.

Despite the numerous parameters that can be set to constrain a rifted margin evolution, FEmargin remains a purely kinematic model with limitations. The exact margin architecture and subsidence history may never perfectly match the data due to the absence of faulting in the model. Fortunately, the amplitude effects of faulting remain local and would therefore not affect the regional calibration. Extension driven by buoyancy upwelling (plume) is limited in FEmargin because the buoyancy induced upwelling deformation mode only affects the mantle and not the upper brittle lithosphere. This limitation may affect the scenarios in which the Karoo volcanic event induces rifting and the breakup of Gondwana. However, an adequate control of the pure-shear and a high buoyancy upwelling rate can mimic extension driven by buoyancy. In addition, variation of density, thermal conductivity or radiogenic heat production are laterally constant in a layer. Consequently, we neglect the effect of crustal and mantle inheritance (depleted or hydrated mantle); such inheritances would affect the geothermal gradient and thus locally heat flows and melt generation due to variations in conductivity or radiogenic heat productivity. The extraction of melt is also limited to the surface or to the underplate, therefore melt emplacement in the continental crust is not possible.

3.2 Available data for calibration

Margin deformation is modelled and calibrated using an extensive dataset available in the study area. These constraints include present-day crustal architecture, thermal calibration, spreading rates, sedimentation rates and melt generation histories.

3.2.1 2D seismic profiles

Available seismic data provide calibration for the thickness of the sedimentary cover (Fig. 4). The stratigraphy was interpreted by Ponte (2018) on the 2D MCS seismic reflection profile located in the northern Mozambique basin (Fig. 1; 4) which was acquired by INP – WesternGeco in 2013.

The ages of the seismic horizons range from 0 to at least 155 Ma. Depth conversion and interpolation of horizons were done using the sonic velocities of several wells in the vicinity of the Beira High (Fig. 1). The sediment thickness ranges from ~12 km in the Zambezi depression to ~ 4 km in the Mozambique distal basin. There are also some indications of volcanism: 1) eroded Karoo basalts (Ponte, 2018, Klimke et al., 2018, Senkans et al., 2019) of Early Jurassic age (~183 Ma), which are thought to be related to the beginning of the Gondwana rifting, and 2) wedges of seaward-dipping reflectors (SDRs) seen on seismic lines which are assumed to be emplaced before the development of the oceanic crust (Fig. 2).

Deep crustal structures (e.g. the Moho) and thus, the margin geometry at crustal scale are not well imaged by the available seismic reflection data. Thus, we combined the interpretations of seismic reflection data with the seismic refraction model of Mueller et al. (2016; 2017) (Fig. 4). Their interpretation is performed along the 530 km long refraction profile 20140010, a NNW-SSE oriented section through the Beira High, which was acquired by the AWI (Alfred Wegener Institute, Helmholtz Centre for Polar and Marine Research, Germany) and the BGR (Federal Institute for Geosciences and Natural Resources, Germany) in 2014 (Jokat, 2014). The root-mean-square (RMS) error of the crustal thickness described in their model for NW-SE profiles located in the Angoche area is estimated for the Beira High area at maximum of 10 % of the Moho depth (~2 km vertically).

3.2.2 Well data

Several wells were drilled in the study area. We used four wells located within 8 to 70 km of the Beira High section and labelled Well 1 to Well 4 (Fig. 4). Temperature data used in this study are mostly

(corrected) bottom hole temperatures and temperature gradients. The comparison between the thermal data and those predicted by the model help us to evaluate our scenarios (see section 4.2).

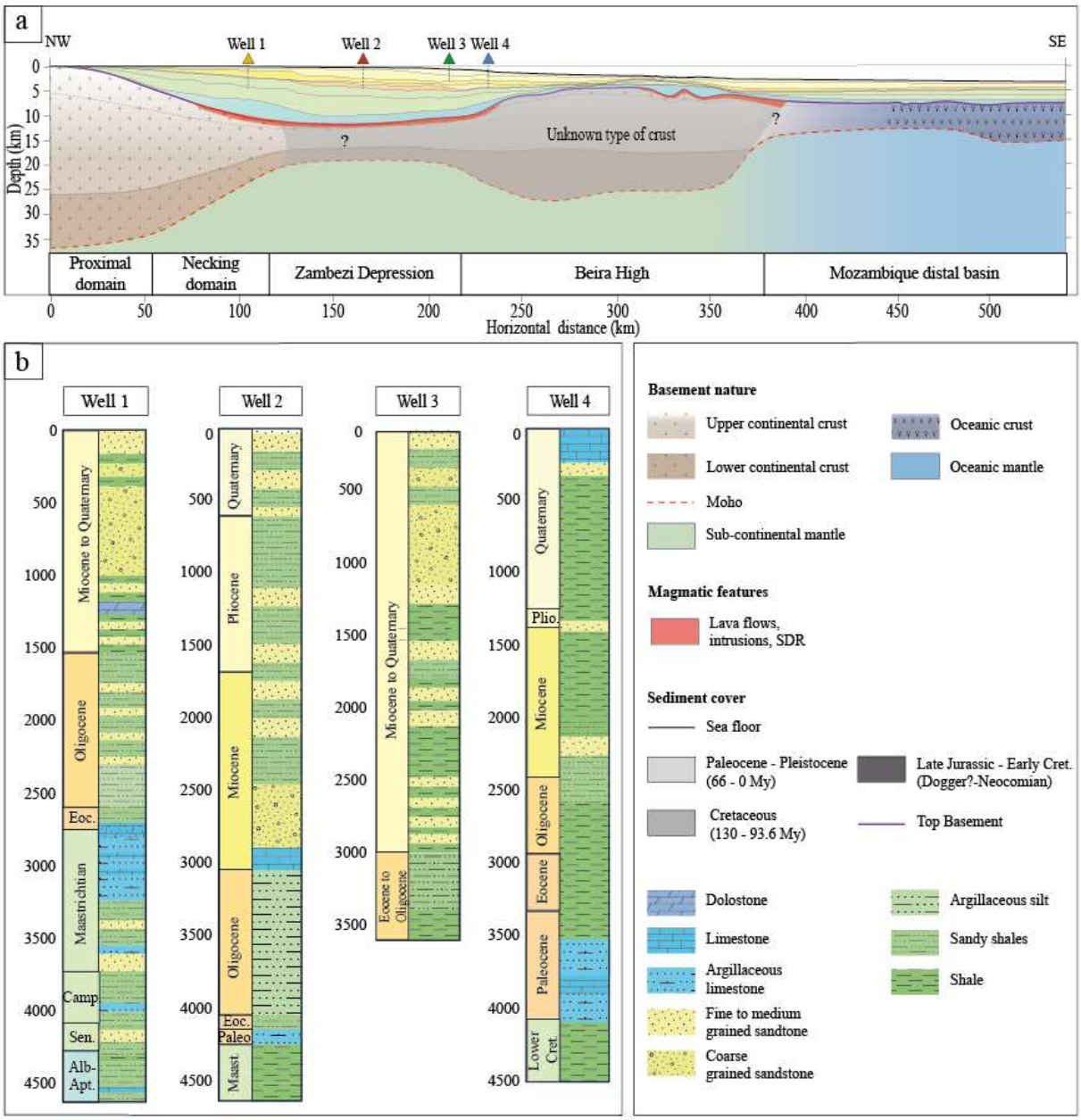

Figure 4: a) *Interpreted seismic refraction profile and projection of the wells used in the study (modified after Mueller et al., 2017). The sedimentary cover is interpreted by Ponte (2018). See location in Fig. 1.* ***b)*** *Simplified lithological facies for the studied wells located in the vicinity of the Beira High.*

3.3 Modelling constraints

3.3.1 Target geometries for the calibration

The crustal architecture of the rifted margin is the main feature used to constrain the kinematic modelling. The model predictions of crustal thickness, bathymetry, top basement and Moho must match the observed present-day geometries (Fig. 4).

The thickness of the continental crust proposed by Mueller et al., (2016, 2017) decreases from more than 37 km in the Mozambique proximal margin to ~8 km within the Zambezi depression (Fig. 4a). The thickness of the unspecified crust is ~20 km in the Beira High and thins to 5-8 km in the Mozambique distal basin (Mueller et al., 2016).

Since it is unlikely that a perfect match between observed and modelled margin geometry will be achieved, we set the maximum vertical and horizontal errors to 2 and 5 km, respectively.

3.3.2 Constraints on the kinematic evolution

i) Total extension and strain rates

We quantify the total extension of the continental crust along the Beira High (Fig. 1) to estimate a first approximate steady strain rate from continental thinning to crustal breakup. Since the crustal structure of the conjugate margin in Antarctica is not well known, the extension amount has only been calculated along the Mozambican margin. The total extension has been estimated using a conservative areal balancing restoration, based on the estimation of the surface of the continental crust on the seismic profile through the Beira High, using an initial crustal thickness of 37 km in the Beira High profile, following Mueller et al. (2017). Knowing the surface of the continental crust and the initial crustal thickness, we determined the initial width of the crust before rifting, enabling us to calculate the total extension. The amount of stretching of the studied rifted margin mainly depends on the nature of the crust in the Zambezi depression and the Beira High. If the Beira High consists of continental crust, (e.g. with a COT location proposed by Mueller et al., 2016; 2017), the total stretching would approximately amount

to 200 km. In addition, syn-rift magmatic activity and the resulting amount of magmatic intrusion in the crust may have a significant impact on the total extension estimated; the presence of magmatic intrusion likely leads to an overestimation of the amount of extension and thus, of strain rates.

The extension rate values depend on the total extension and the duration of rifting. However, uncertainties exist about breakup ages; we chose a breakup age at 157± 3 Ma (Fig. 2). Assuming the initiation of rifting at 183 Ma and the oceanic accretion beginning at 157 Ma, a mean extension rate of 7.7 mm/yr is obtained in the Beira High margin. However, this approximation should be used with caution due to the uncertainties related to the duration of rifting, the COT location and syn-rift magmatic activity. This value is nonetheless useful as an initial first guess for modelling, which is then refined with the quantitative calibration of the observed crustal geometries and age of breakup.

Following the breakup and during seafloor spreading, we constrain our models based on the interpretation and location of magnetic anomalies on the modelled section. Leinweber and Jokat (2012) and König and Jokat (2010) proposed half-spreading rates of 23.5 mm/yr from M26n.1n (155 Ma) to M22n.1n (149 Ma), and of 21 mm/yr from M22n.1n (149 Ma) to M12.r.1r (138 Ma). We use a mean half-spreading rate of 22 mm/yr until 140 Ma, after which the entire model cools to equilibrium until present-day. This late thermal subsidence is applied to all models due to width limitations in FEmargin and is characterized by a zero spreading rate and no active upwelling. We assume that the advection of temperature during seafloor spreading does not affect the proximal margin. With this approach, the 183-140 Ma extension rates applied in FEmargin are similar to the ranges of values proposed by Clark (2018).

ii) Sedimentation and associated subsidence history

Coupling the lithosphere evolution with sedimentation is important for the prediction of accurate thermal histories at rifted margin (Callies et al., 2018). The sedimentary filling is constrained by using seismic and well interpretation (Fig. 2; Fig. 4) and values of mean sedimentation rates found in the literature (see below).

The initial Gondwana rifting led to a rapid subsidence during crustal stretching before the breakup (Mahanjane, 2012, Castelino et al., 2015). An Upper Jurassic transgression is identified in the Mozambique Basin (Mahanjane et al., 2014). This transgression resulted in the deposition of about 3 km of Jurassic to Lower Cretaceous sediments localized mostly in the Zambezi depression above Karoo volcanics (Mahanjane, 2012; Castelino et al., 2015). The Jurassic sediments are not distributed evenly in the study area (Mahanjane, 2014). A thin layer of Lower Cretaceous sediments on the Beira High suggests that it may have already been a high (Mahanjane et al., 2014), separating the Zambezi depression from the future offshore basin. Most studies agree on an onset of sedimentation in the Limpopo plain and North Zambezi depression during the Late Jurassic to Early Cretaceous (at least Tithonian until Valanginian) (Salman and Abdula, 1995; Thompson, 2017; Baby, 2017) with sandstones forming the continental Red Beds Formation (Fig. 2).

In the central Mozambique Basin, the Top Neocomian to Albian deposits unconformably lay on the Valanginian sediments and are characterized by continental sands onshore (Sena Formation) and marine shales on the shelf (the Lower Domo Formation) (Mahanjane et al., 2014; Baby, 2017; Ponte, 2018; Thompson, 2017) (Fig. 2). This Lower Domo Formation represents a major transgression of the shelf (Thompson, 2017). During the Aptian and Albian, about 2 km of sediments were deposited (Mahanjane et al., 2014).

The sedimentation rates increased in Aptian-Albian times (Mahanjane et al., 2014). The Upper Cretaceous deposits are characterized by the Domo sands Fm (sandstones alternating with black shales) and Upper Domo Fm (shales) (Nairn et al., 1991; Key et al., 2008; Mahanjane et al., 2014; Ponte, 2018) (Fig. 2). Thermal relaxation began at the end of the Cretaceous and is marked by a major marine transgression, which is responsible for the deposition of the Grudja Formation (alternating shales and glauconitic siltstones) (Mahanjane et al., 2014; Thompson, 2017). About 2 km of sediments are deposited from Middle to Late Cretaceous in the central Mozambique Basin (Mahanjane et al., 2014).

From the Paleocene to Eocene, a major flooding event associated with a peak temperature around the Paleocene Eocene Thermal Maximum (PTEM) (Röhl et al., 2007) is responsible for the deposition of a shallow-marine carbonate platform belonging to the Upper Grudja and Chéringoma formations. From Oligocene and throughout the Neogene, the margin acquired a prograding morphology along with the Zambezi delta initiation (Baby, 2017; Ponte, 2018). According to Salman and Abdula (1995), 5 km of sediments were deposited during the Cenozoic.

iii) Timing and evidence of magmatism

During thinning of the lithosphere, the upwelling asthenospheric mantle decompresses and may partially melt (McKenzie and Bickle, 1988; Bown and White, 1995). In FEmargin, melt generated from decompression melting can be directly extracted at the surface or underplated, but it can also be retained in the mantle. The volume of melt produced during decompression melting is function of the width of the pure-shear domain, the strain rate and the buoyancy upwelling rate. The parameters characterizing melt production and extraction must therefore be calibrated when investigating the nature of the crust in the Beira High. For this, we use the timing, location and volume of magma (Mueller et al., 2016, 2017; Ponte, 2018; Mahanjane, 2014) (Fig. 1, 2 and 4).

Some of the kinematic reconstructions that we model include the presence of an oceanic crust underlying the Beira High and/or the Zambezi depression. These models directly affect the half-spreading rates and the assumed mantle buoyancy, which may be higher than those proposed for magma-poor margins (Jeanniot et al., 2016). Increase in melt production can be obtained by accelerating the lithosphere thinning.

The melt duration is calibrated against the magmatic events described in the literature (Mueller et al., 2016, 2017; Ponte, 2018; Mahanjane, 2014) (Fig. 2). Regarding the Karoo-Ferrar (LIP) igneous event, sills and lava flows were deposited in the northeastern margin of central Mozambique. SDR emplacement has been dated from 177 ± 3 Ma to 157 ± 3 Ma by Mueller et al. (2017), who proposed another

magmatism phase between 177 Ma and 164.1 Ma along the central Mozambique margin. This magmatism phase may be at the origin of a high velocity body within the Zambezi depression and offshore of the Angoche margin (Leinweber et al., 2013; Mueller et al., 2017). At the northwestern flank of the Beira High and in the offshore Zambezi margin, Mueller et al. (2017) suggest a rift volcanism stage between 166.8 Ma and 164.1 Ma. This volcanic event preceded the formation of the oldest oceanic crust, estimated in their paper around 164 Ma. During this stage, a flow of acid lavas (the Lupata rhyolites) is described in the Zambezi depression at 166 ± 10 Ma (Flores, 1964). A late magmatic stage related to seafloor spreading is dated at 157 ± 3 Ma (Mueller et al., 2017). The southward migration of the spreading center may be responsible for the subsequent decrease of magmatism in the Central Mozambique margin (Mueller et al., 2017).

3.4 Application to the Mozambique rifted margin: modeling scenarios

3.4.1. Model timing and physical parameter setup

Each modelled scenario is characterized by several deformation steps approximating the rifting of Gondwana from Early Jurassic to present:

- Toarcian to Late Toarcian-Early Aalenian (183 – 178 Ma) corresponds to an early rifting stage characterized by a slight asthenospheric upwelling over a wide zone;
- Late Toarcian-Early Aalenian to Late Bathonian (178 – 166 Ma) is defined by the emplacement of magmatic features and by the onset of thinning localized in the future Zambezi depression (Mueller et al., 2017);
- Late Bathonian to Late Callovian (166 – 161 Ma) is characterized by the onset of southward migration of deformation and thinning in the future Beira High area;
- Late Callovian to Late Oxfordian (161 – 157 Ma) corresponds to the localization of the deformation south of the Beira High and the transition to steady state accretion of oceanic crust;

- Late Oxfordian to Late Neocomian (157 – 140 Ma) led to the full development of oceanic crust;
- From 140 Ma to present is characterized by thermal subsidence only due to the software width limitation.

The model input parameters are summarized in Table 1. Assumptions were made regarding the lithologies of the sedimentary, crustal and mantle units. Reasonable ranges of density, radiogenic heat production and thermal conductivity values were assigned to each layer according to the literature (Pasquale et al., 2014, Nemcok and al., 2017, Hasterok et. al 2017 and Allen and Allen, 2013) (Table 1). These parameters are identical in all scenarios.

Model Parameter	Variable	Value	Units
Parameters that are identical in all scenarios			
Initial lithosphere thickness	aT	120000	m
Lithosphere thickness for a linear oceanic geotherm	aK	100000	m
Heat capacity	Cpm	1180	Kg.m2/K/s²
Latent heat fusion	LF	400000	J/kg
Thermal expansion coefficient	thermalExp	3.28e-5	
Entropy difference	DS	249.066002	J/kg/K
Gravity accceleration	g	9.81	m/s²
Initial percentage of clinopyroxene in mantle	Mcpx	0.16	%
Base lithosphere temperature	Ta	1330	C
Model depth	aM	600000	m
Distance resolution	dx	5000	m
Depth resolution	dz	1250	m
Initial sediment thickness	tsed	0	m
Initial upper crust thickness	tuppercrust	12500	m
Initial middle crust thickness	tmiddlecrust	15000	m
Initial lower crust thickness	tlowercrust	8750	m
Initial continenal crust thickness	tcrust	36250	m
Surface temperature	Ts	25	C
Sediment radiogenic heat productivity	Hsed	1.0e-6	W/m3
Volcanic radiogenic heat productivity	Hv	0.1e-6	W/m3
Upper crust radiogenic heat productivity	Huc	2.7e-6	W/m3
Middle crust radiogenic heat productivity	Hmc	0.9e-6	W/m3
Lower crust radiogenic heat productivity	Hlc	0.3210-6	W/m3
Mantle radiogenic heat productivity	Hm	0.09e10-6	W/m3
Sediment thermal conductivity	ksed	2.35	W/m.K
Oceanic crust thermal conductivity	kv	2	W/m.K
Upper crust thermal conductivity	kuc	2.6	W/m.K
Middle crust thermal conductivity	kmc	2.2	W/m.K
Lower crust thermal conductivity	klc	2.2	W/m.K
Mantle thermal conductivity	km	3.5	W/m.K
Density air	pa	0	kg/m3
Density water	pw	1040	kg/m3
Density sediment	psed	2100	kg/m3
Density volcanic layer	pv	2850	kg/m3
Density upper crust	puc	2690	kg/m3
Density middle crust	pmc	2910	kg/m3
Density lower crust	plc	2950	kg/m3
Density mantle	pm	3330	kg/m3
Sedimentation rate	?	_	km/Myr
Modifiable parameters that may be different in each scenarios			
Pure-shear width	W	_	km
Half-spreading rate	Vx	_	km/Myr
Additionnal upwelling rate	Vz	_	km/Myr
Buoyancy ratio	Vz/Vx	_	_
Horizontal coordinate	X	_	km
Vertical coordinate	Z	_	km
Migration factor	fm	_	_
Melt extraction/underplated width	_	_	km
Melt threshold prior extraction	Fret	_	%
Melt retained in mantle	?	_	%
Melt being underplated	?	_	%

Table 1: *Table of physical and thermal parameters and constants applied in this study.*

Sedimentation rates are identical in all models. From 172 Ma to 140 Ma, the sedimentation rate is calculated based on the 3 km of sediments observed in the Zambezi depression (Mahanjane, 2012; Castelino et al., 2015) that are covered by 2 km of sediments during the Aptian and Albian (Mahanjane, 2014). During the Cenozoic, the sedimentation rate is calculated based on the 5 km of deposits (Salman and Abdula, 1995) observed along the first 200 km of the profile, reproducing the shallow-marine carbonate platform from Paleocene to Eocene, followed by the prograding morphology of the Zambezi depression from Oligocene to Neogene (Baby, 2017; Ponte, 2018).

The pure-shear width (Table 1) remains similar in the scenarios involving a continental origin for the Beira High. However, varying the half spreading rate and deformation width or the melting parameters (buoyancy upwelling rates, percentage of melt retained in the mantle but also the location, width and percentage of melt extruded and underplated) change significantly the resulting geometries in the scenarios that involve magmatic underplating or an oceanic origin for the Beira High. In all models, the melt initiation age coincides with the melt extraction age. An active upwelling (i.e. buoyancy) is required in every modelled scenario to model the lava flows and SDR observed in the Zambezi depression (see 4.1.1 and appendix B).

3.4.2. Models testing the continental or oceanic origin of the Beira High and Zambezi depression

Due to the debated nature of the crust underlying the Beira High and Zambezi depression, the position of the COT is uncertain, which gives flexibility in constraining the early rift stage in the models. The nature of the crust within the Beira High and/or the Zambezi depression might be either continental, oceanic or in transitional.

We formulated 3 kinematic model scenarios:

- Model 1: the Beira High and the Zambezi depression are underlain by continental crust.
- Model 2: the Beira High consists of continental crust and the Zambezi depression has an oceanic origin.
- Model 3: the Beira High and the Zambezi depression have an oceanic origin.

These scenarios do not constitute an exhaustive list but are end-members of possible crustal nature and thermal evolutions for the Mozambique rifted margin.

3.4.3. Models testing the presence or absence of underplated material within the Zambezi depression

Besides the uncertainties concerning the COT location, anomalously high P-wave velocities (> 7.0 km/s) are reported in the study area (Leinweber et al., 2013; Mueller et al., 2016, 2017). The nature of these high velocity bodies is debated. Some authors interpret this feature as accreted mafic material underplating the continental crust during thinning (Leinweber et al., 2013; Mueller et al., 2016, 2017). This underplating is a typical characteristic of volcanic-rich margins (Kelemen and Holbrook, 1995; Menzies et al., 2002; Geoffroy, 2005, 2015; Gernigon et al., 2005; Meyer et al., 2007). Others interpret the high velocity bodies as intrusions of sills in the continental crust (White et al., 2008), or as volcanic material emplaced in an oceanic context (Bauer et al., 2000).

We simulate the extrusion to the surface and/or the underplating of a certain amount of melt, which was produced within the Zambezi depression (Leinweber et al., 2013; Mueller et al. 2016, 2017) to understand its impact on the thermal history of the continental crust. This leads to the subdivision of model 1 into 3 sub-models respectively characterized by an increasing amount of extracted melt (Fig. 5):

- Model 1a: the Beira High and Zambezi depression are underlain by continental crust.
- Model 1b: the Beira High and Zambezi depression consist of continental crust with magmatic underplating in the Zambezi depression.
- Model 1c: the Beira High and Zambezi depression consist of continental crust characterized by a magmatic underplating.

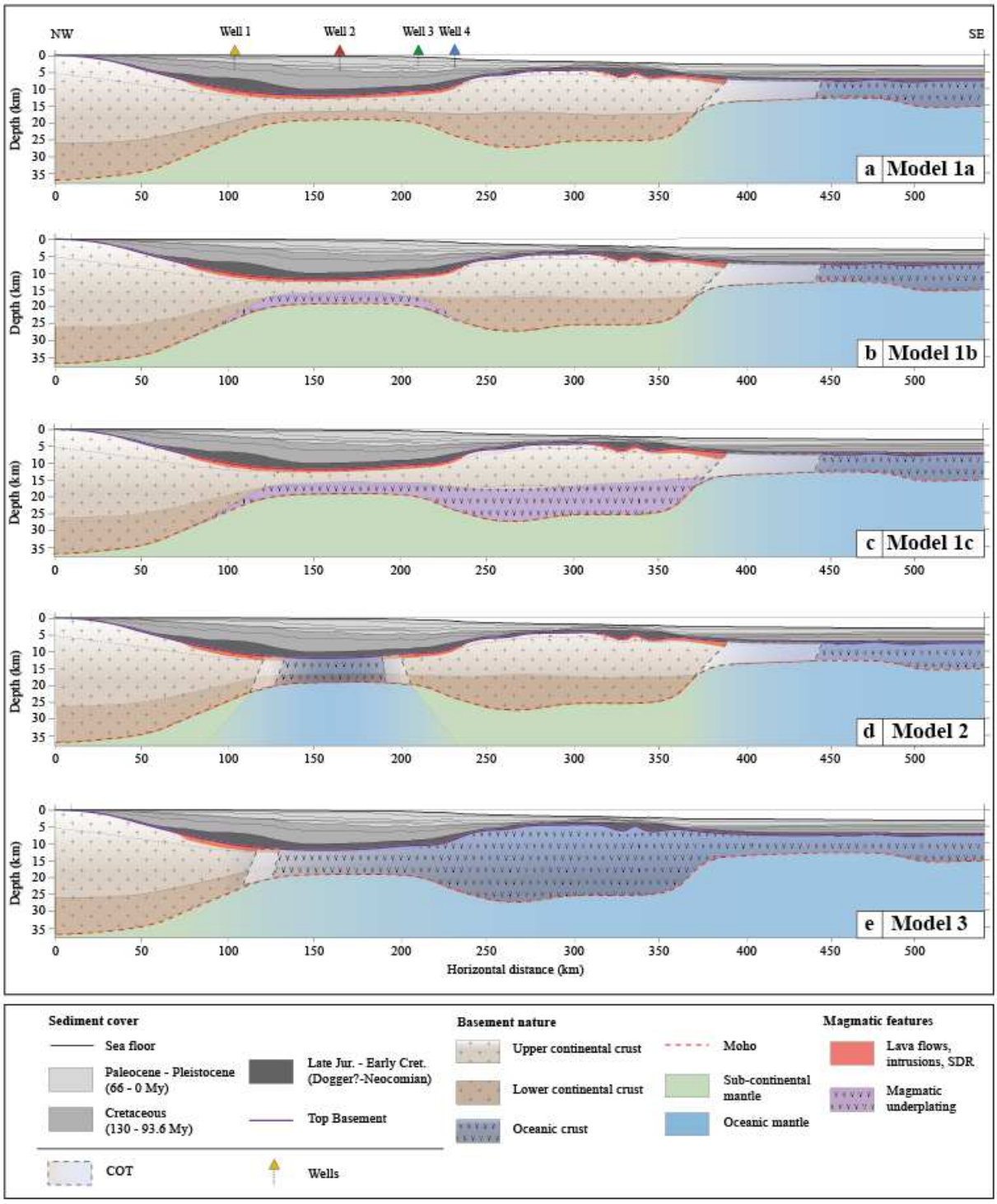

Figure 5: *Schematic representations of the five tested models. The origin of the crust in the Zambezi Depression may be* ***a)*** *entirely continental without magmatic underplating (Model 1a),* ***b)*** *continental with*

magmatic underplating in the Zambezi depression (modified after Mueller et al., 2017) (Model 1b), ***c)*** *continental with magmatic underplating in the Zambezi depression and Beira High (Model 1c),* ***d)*** *oceanic with a continental origin for the Beira High (Model 2),* ***e)*** *entirely oceanic with an oceanic origin the Beira High (Model 3).*

4. MODELLING RESULTS

The five modelling scenarios shown in Fig. 5 allow us to test the influence of the crustal nature and near-margin magmatic processes on the thermal history of the sediments of the Mozambique margin. The calibration of the deformation for each modelling scenario is shown in appendix A. In order to fit the crustal architecture, the five models, 1a, 1b, 1c, 2 and 3 differs more or less from each other regarding the extension and upwelling rates, pure-shear width, continuous migration of the flow fields and melt extraction axes. However, they all share the same sediment deposition history and timings of deformation.

For each modeling scenario, the predicted rifted margin architecture and thermal history are compared and quantitatively calibrated against the present-day crustal geometries of the Mozambique margin. The mean error between the modelled geometry and the input must be as low as possible for a meaningful interpretation of the thermal results. Once the geometries are matched to the desired degree, we reduce the misfit between the thermal data observed at the wells and the computed thermal predictions by updating the buoyancy upwelling rates and parameters controlling melt extraction. The parameters controlling melt extraction are numerous, including the percentage of melt being retained in the mantle and the percentage, width, and location of the melt being underplated or extracted at the surface. The fit between predicted and measured thermal results may be more or less satisfying depending on the scenario.

The modelled lithosphere and asthenosphere evolutions of each scenario are displayed in Fig. 6 from 183 Ma until 140 Ma for a better overview.

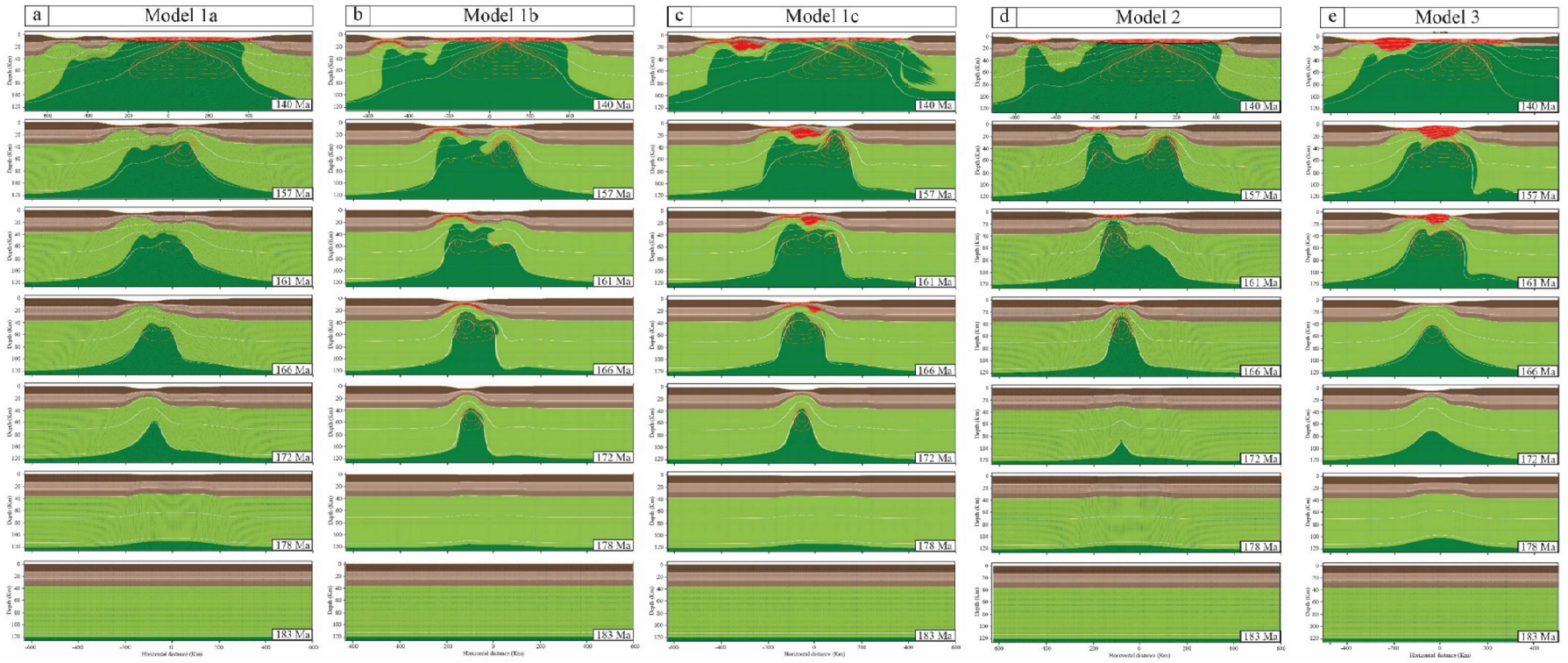
a
Model 1a
b
Model 1b
c
Model 1c
d
Model 2
e
Model 3
140 Ma
157 Ma
161 Ma
166 Ma
172 Ma
178 Ma
183 Ma
Depth (Km)
Horizontal distance (Km)

Figure 6: *Modelled lithosphere and asthenosphere evolutions obtained from* ***a)*** *model 1a,* ***b)*** *model 1b,* ***c)*** *model 1c* ***d)*** *model 2 and* ***e)*** *model 3. All models run from 183 Ma until present-day. Seven stages are shown at times 183, 178, 172, 166, 161, 157 Ma (Break-up age) and 140 Ma. The asthenosphere is in dark green, the lithosphere in light green and lower to upper crust are in shades of brown. Volcanic Features (SDR, lavas flows, underplating and oceanic crust) are in red. White solid lines are isotherms in °C (from top to bottom: 300, 600, 900, 1100, 1300) and red solid lines are melt fraction (3% interval).*

4.1. Modeled deformation and timing of breakup

4.1.1 Reference Model 1a: the Beira High and the Zambezi depression are underlain by continental crust.

The evolution of the lithosphere and asthenosphere in model 1a is shown in Fig. 6 from 183 Ma to 140 Ma. A first regional pure-shear deformation is applied from 183 to 178 Ma, with a deformation width of 300 km and a half extension rate of 4.5 mm/yr. From 178 Ma until 157 Ma, the pure shear width narrowed between 65 km and 40 km while the half extension rates is increased from 4.5 mm/yr to 10 mm/yr. In addition, an active upwelling of about 7 mm/y is applied within the future Zambezi depression between 178 and 164, to ensure early melt generation at about 166 Ma. This melt is important to simulate SDRs and/or lava flows at the top of the Zambezi depression basement (Mahanjane, 2012; Mueller et al., 2017; Ponte, 2018; Senkans et al., 2019), and volcanic intrusions and/or SDRs south of the Beira High (Ponte, 2018; Senkans et al., 2019). In the case where model 1a would not include melt (Model 0, Appendix B), no melt is produced prior to break-up. Higher extension rates throughout rifting are also not compatible with the calculated amount of extension, so that the only way to ensure melting as the observation suggest is to start early decompression melting by increasing buoyancy.

Breakup of continental crust occurs south of the Beira High around 157 Ma because of an increase in extension rate and more localized deformation. The development of the oceanic crust is

constrained by a pure-shear deformation width of 25 km and a half-spreading rate of 22 mm/yr from 151 Ma.

The predicted present-day rifted margin architecture is compared with the observed geometries in Fig. 7. The match between the predicted present-day model and the observed architecture is satisfying NW of the COT (the shift being of about 5 km vertically and 2 km horizontally). The misfits between the model and the input geometries increase SE of the Beira High, in the oceanic domain. This mismatch may be due to the low density of deep-sea sediments (Nemcok et al., 2017) which cannot be computed due to a constant density value prescribed in FEmargin for the entire sedimentary infill.

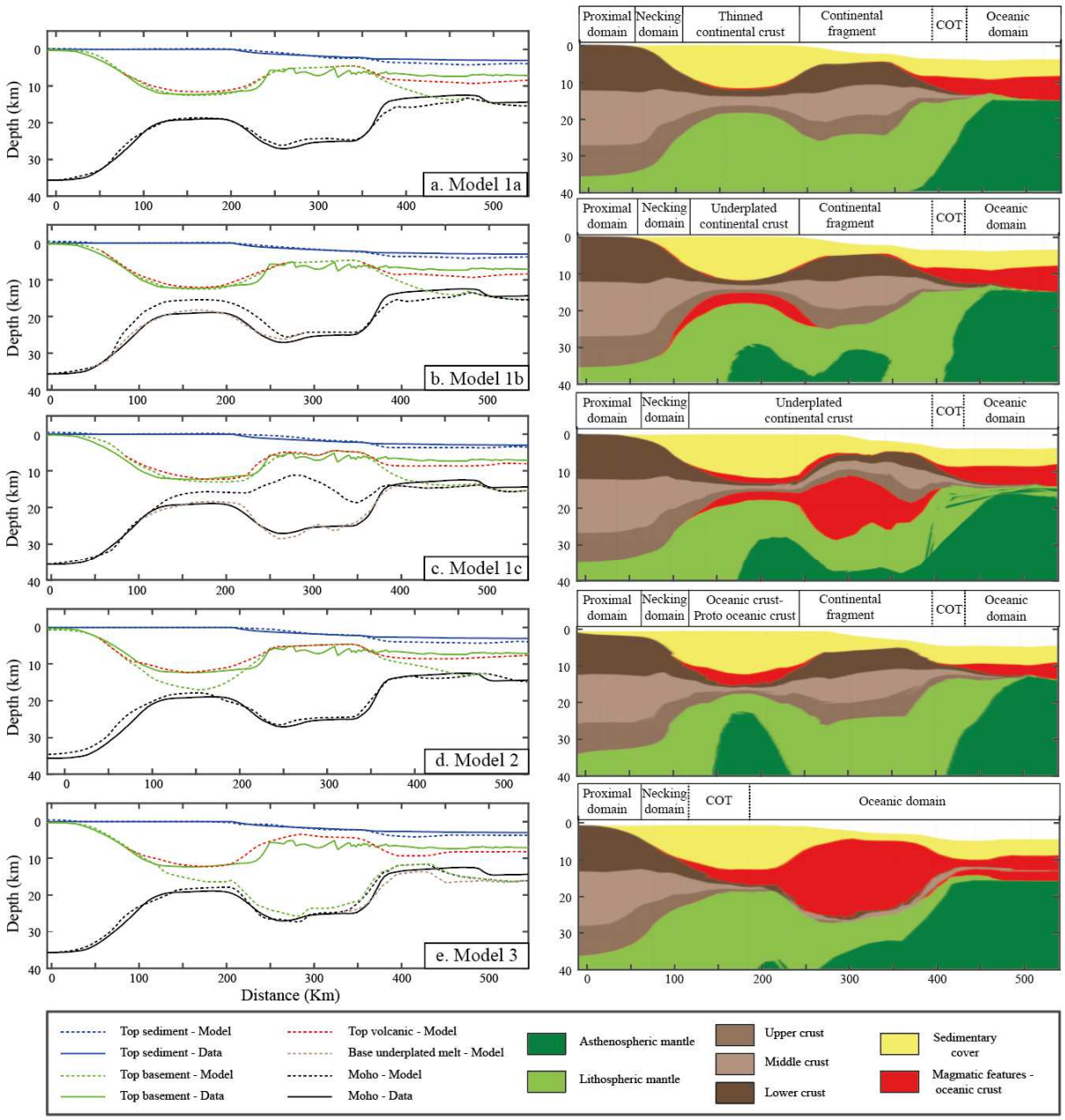

Figure 7: *Present-day margin architecture and associated calibration for model 1a, model 1b, model 1c, model 2 and model 3 of the cross section through the Zambezi Depression and the Beira High. For each model, four predicted present-day horizons (Moho, top Basement, top volcanic and top sediment) are compared to those from Figure 4.*

4.1.2 Model 1b: the Beira high and the Zambezi depression consist of continental crust with magmatic underplating.

The Beira High is considered as a stretched continental ribbon as in model 1a, but magmatic material is underplated below the Zambezi depression. The prescribed evolution history of model 1b remains the same as in 1a for post-rift deformation steps (Fig. 6). The pure shear width and half extension rate are close to the ones applied in model 1a. However, this model assumes higher buoyancy upwelling rates (minimum 25 mm/yr instead of 7.5 mm/yr in model 1a) during the deformation steps affecting the Zambezi depression (from 178 Ma to 166 Ma). This increase in buoyancy upwelling rates results in an increase of the melt production, which is underplated underneath the continental crust of the Zambezi depression starting predominantly at 176 Ma, in agreement with Mueller et al. (2017). From 166 to 164 Ma, the deformation migrates southward to simulate the rift jump south of the Beira High. Crustal breakup is set south of the Beira High at around 157 Ma. The deformation then evolves as in model 1a, with seafloor spreading from 157 Ma.

The match between predicted and observed geometries remains good (less than 5 km shift vertically and 2 km horizontally) (Fig 7). A magmatic underplate about 150 km wide and 3 km thick is modelled within the Zambezi depression.

4.1.3 Model 1c: the Beira High and the Zambezi depression consist of continental crust characterized by a magmatic underplate.

In this model, the magmatic contribution is higher than in models 1a and 1b. The magmatic underplate that developed from 172 Ma to 166 Ma in the Zambezi depression (model 1b) continues towards the south, resulting in a thick magmatic underplate below the Beira High (Fig. 6). The asthenospheric upwelling rates are predicted to be higher than in model 1b, especially from 168 Ma onward. Due to the high melt production, the lava flows in the Zambezi depression and north of Beira High are thicker in this model than in models 1a and 1b. As in model 1b, the lithosphere-asthenosphere

boundary rises to less than 40 km depth in the Zambezi depression. The deformation then migrates towards the south, leading to break up around 157 Ma.

The present day calibration between observed and modelled architecture remains good (Fig. 7), despite some difficulties to match the geometry of the Moho below the Beira High. Indeed, maximum asthenospheric upwelling rate values of 55 mm/yr are prescribed instead of 35 mm/yr in model 1b) in order to produce enough melt to reach a magmatic underplate of about 10 km thickness.

4.1.4 Model 2: the Beira High consists of continental crust and the Zambezi depression has an oceanic origin.

In this model, we prescribe a narrow pure-shear domain of extension (40 km) initiated at 172 Ma in the Zambezi depression associated with high asthenospheric upwelling rates (20 mm/yr in average) and spreading rates of maximum 12 mm/yr. The combination of a narrower domain of pure shear, a greater half extension rate and buoyancy upwelling rates induce a faster thinning of the continental crust and lithosphere, and thus an earlier crustal breakup in the Zambezi depression at around 164 Ma. This corresponds to the breakup age observed in the Angoche region (Mueller and Jokat, 2017). This first formed rift became an extinct mid-ocean ridge when the deformation moved toward the SW from 164 Ma to 157 Ma, coinciding with the age of the breakup south of the Beira High.

The model does not match well with the present-day architecture of the Zambezi depression (the vertical misfits are larger than 5 km). The short timing between the onset of rifting and breakup, as well as the narrowness of the Zambezi depression, make it difficult to form a thick oceanic crust with no continental crust remnant (Fig. 7).

4.1.5 Model 3: the Beira High and the Zambezi depression have an oceanic origin.

Model 3 is an end-member case, which requires a large amount of melt to build the 20 km thick crust of the Beira High. In order to rapidly thin the continental crust, the pure shear width is assumed

narrower than in previous models (W ≤ 50 km from 178 to 140 Ma). In addition, half extension rates are slightly higher (maximum 12 mm/yr from 178 to 161 Ma instead of a maximum of 10 mm/yr in previous models). Asthenospheric upwelling rates are much higher from 166 Ma on (maximum 95 mm/yr instead of 55 mm/yr in model 1c) in order to produce enough melt to reach the observed crustal thickness. Following the southward migration of the deformation, the development of the thick oceanic crust led to the formation of an entirely igneous Beira High. The deformation then migrates south. The crustal architecture of the margin is more difficult to match in this scenario than in models 1a and 1b (Fig. 7).

4.2. Predicted thermal histories and calibration of models

The predicted and observed temperature at the wells for each modelled scenario are shown in Fig. 8. The mismatch between the modelled temperatures and data observed in the onshore Well 1 is similar in all models (20 to 30°C). All models overestimate the temperature in the sedimentary layers in this area, and model 1b provides a slightly better fit (20°C) with borehole temperature data.

Elsewhere, temperatures fit better to data. In particular, there is a small error range (lower or equal to 10°C) in the continental crust models (1a, 1b and 1c). The error range seems to increase with the magmatic contribution, especially in wells 2 and 3 located in the hyper-thinned domain of the Zambezi depression. In model 3, the Well 4 is located on an oceanic Beira High and provides a higher mismatch (more than 10°C).

The temperature predicted in continental models 1a, b and c seems to better match the temperature data. In addition, the misfit in present-day calibrations (Fig. 8) remains mostly lower than 20°C in well 2, 3 and 4. This may have 2 possible causes. Callies et al. (2008) suggest that the present-day thermicity is no more affected by rifting processes. The second explanation may derive from the lack of faulting in FEmargin, and the uniform thinning of the continental crust, which enable the lower and/or middle crustal flow with respect to the more rigid upper crust (Brune et al, 2017).

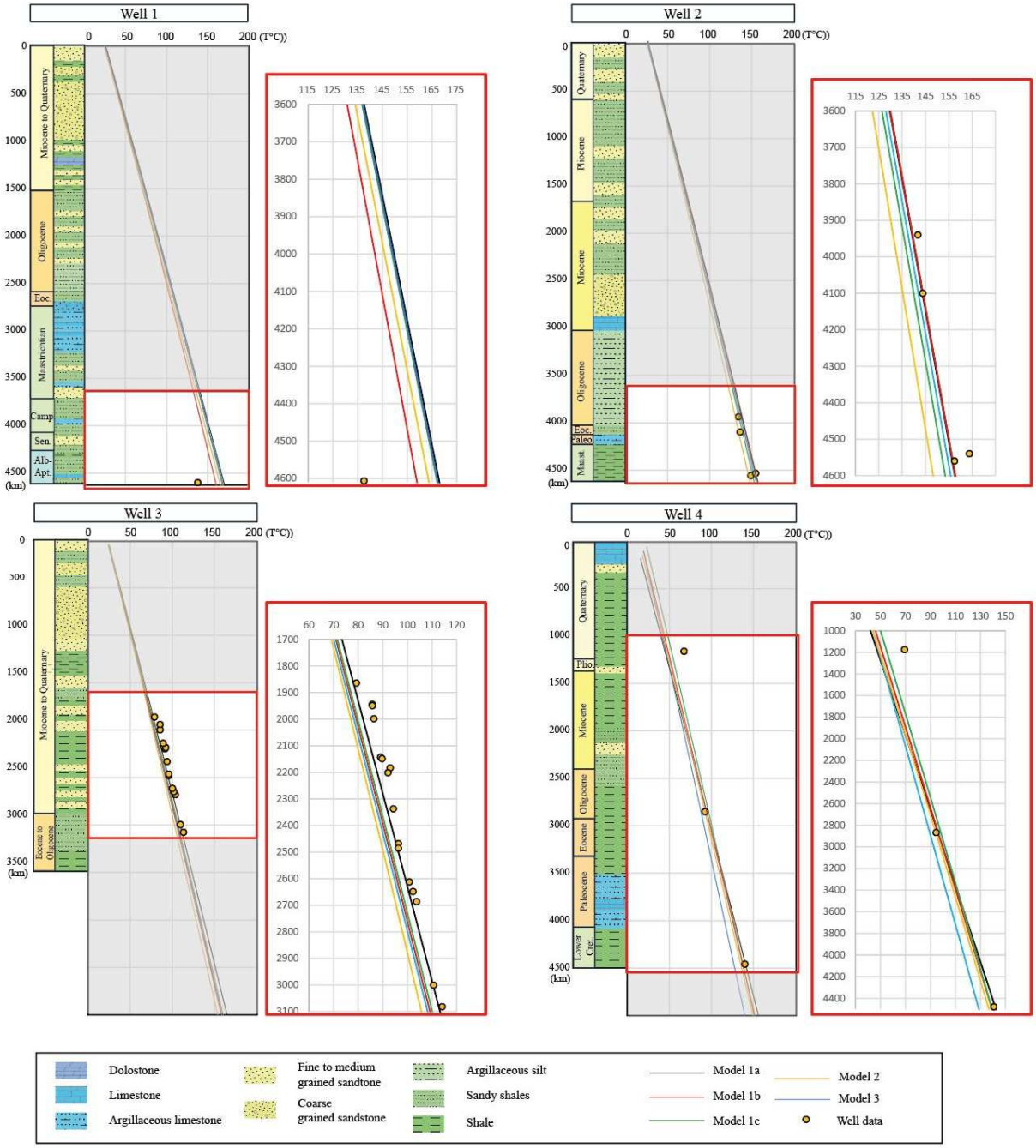

Figure 8: *Comparison of predicted present-day temperature - depth profiles at 4 well locations (Well 1 to 4) with measured temperatures from each model (see Fig. 1, 4 for location).*

5- DISCUSSIONS

Our study aimed to unravel the nature of the crust in the Zambezi depression and in the vicinity of the Beira High. The calibration uncertainty variations are discussed regarding the role of the lack of crustal heterogeneities in our modelling. Then, the temperature history is examined with the aim to answer our initial issue, which is the nature of the crust in the Zambezi depression and the Beira High. Finally, we discuss why a rift jump had occurred in this region.

5-1 Calibration uncertainties and sensitivity analysis

The initial parameters used as mean values in this study are from Pasquale et al., 2014, Hasterok et al., 2017, and Allen and Allen, 2013. However, a large range of values characterizes these parameters, especially the conductivities and radiogenic heat production. These two thermal parameters play a key role in the temperature evolution of a passive margin but they are set per layer in our modelling approach. Therefore, lateral variation caused by magmatic intrusions within the crust would not be taken into account while they would inevitably locally affect the radiogenic heat production and conductivity, thus the present-day temperature.

To quantify the thermal response associated with the variation of model parameters, we performed a series of numerical experiments on the five-modelled scenarios 1a, 1b, 1c, 2 and 3. We tested the present-day temperature sensitivity to 10% variations of the radiogenic heat productivity and thermal conductivity. The results are shown in Appendix C and D. The variation of conductivities and radiogenic productions don't lead to major variations of temperature but show that an intermediate value of these parameters is most appropriate to calibrate the whole set of well data.

The oceanic models 2 and 3 show a bigger mismatch with the data, especially in the wells 2 and 3. These models appear to be colder than the data, even with a higher conductivity or a lower radiogenic

heat production. This can be explained by a thinner (if not non-existent) continental crust in these scenarios and thus a lower radiogenic heat production. In these area, the presence of a continental crust might be necessary to match the thermal data. Therefore, we can favour the continental models (1a, 1b and 1c).

This sensitivity analysis does not present a significant mismatch with the data, but it gives a general behavior in response to the variation of chosen parameters. Another scenario hypothesis may have led to higher mismatches with the data, but we choose to keep the models simple for the software potential and to focus on a variation of parameters (conductivity and radiogenic production) which are directly used in the thermal equations.

5-2 Thermal evolution of the Mozambique rifted margin.

The five modeled scenarios 1a, 1b, 1c, 2 and 3 show that the nature and architecture of the crust in the Zambezi depression and the Beira High have a rather small impact on the present-day thermal state of the margin, as it is seen with the wells temperature. In contrast, the thermal evolution, and therefore the heat flow history in the sedimentary basin, will likely be affected by strong upwelling during the formation of the rifted margin.

As an example, we tracked the heat flow evolution calculated in model 1a at the base of the sedimentary cover within the main structural domains during the entire margin deformation. Fig. 9 shows the heat flow evolution at seven locations along the margin profile. The heat flow varies along with the main structural domains across strike. It reaches 95 mW/m² in the thinned continental domain (e.g. at the locations of wells 2 and 3) and rises to ~140 mW/m² in the COT, and to ~160 mW/m² in the oceanic domain. The heat flow does not exceed 70 mW/m² in the necking domain (e.g. at the location of Well 1) and 55 mW/m² in the proximal domain, where it is mostly controlled by the radiogenic heat production of the continental crust. The oceanward migration of the heat flow peak is a consequence of the rift center

migration. After break-up, the lithosphere beneath the margin cools and thermal subsidence occurs. This leads to a considerable drop of heat flow in oceanic domains, away from mid-ocean ridge. Indeed, the heat flow predicted in the oceanic domain rapidly decreases from the highest value to the lowest. A possible explanation is that there is no remnant continental crust left to maintain a sufficient radiogenic heat production towards the oceanic domain.

Further investigation of past thermal indicators in the study area and their comparison with the calculated ones from each models may be a useful progression from this work.

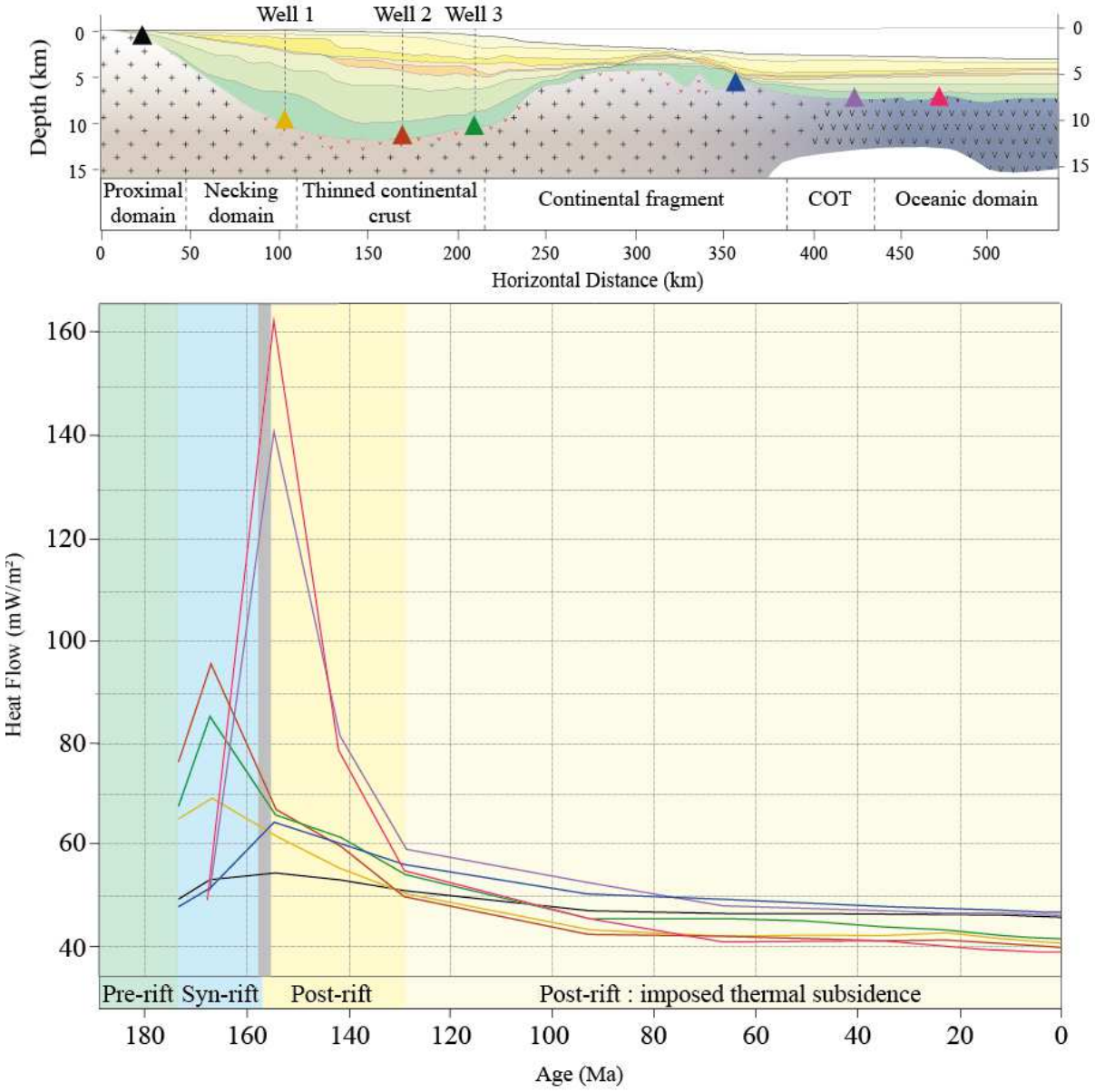

Figure 9: *Predicted heat-flow evolution of Model 1a since 183 Ma until present-day for 7 locations along the modelled margin. Each curve corresponds to a well of the same color code. The mean heat flow values rise from the proximal domain to the oceanic domain. Note the delay between the heat-flow maximum predicted in the Zambezi depression and those of the distal domains; this delay is an illustration of the oceanward deformation migration. Present-day heat flow values ranges between 40 and 50 mW/m².*

5-3 Crustal nature of the Beira High and the Zambezi depression

We favour a continental nature of the crust below the Beira High and the Zambezi Depression (Model 1a, 1b or 1c) which is in agreement with recent studies (Mahanjane, 2012; Senkans et al., 2019; Mueller et al., 2016, 2017). Model 1a results are not consistent with other studies. Indeed, the magmatic activity in the Mozambique basin is responsible for the formation of SDRs in the Angoche margin (Leinweber et al., 2013; Mueller et al., 2017; Ponte, 2018; Senkans et al., 2019). Ponte (2018) suggests also the presence of SDRs in the Zambezi depression from seismic interpretation.

The present-day margin architecture of Model 1b and 1c were easier to calibrate compared to those of oceanic models 2 and 3. Moreover, they provide satisfying thermal calibrations. The Mozambique rifted margin belongs to the category of magma-rich margins that are characterized by an intense magmatic activity. Given all the evidence of magmatic activity in the surrounding areas as well as the negative magnetic anomaly in the Zambezi depression (Leinweber and Jokat, 2012; Mueller et al., 2016; 2017), intrusions and magmatic underplating are most likely to be present in the studied profile. The volume of melt underplated or intruded in the vicinity of the Beira High remains nevertheless unknown.

The presence of continental crust below the Zambezi depression and the Beira High has a direct implication on the kinematic plate reconstruction, and it invalidates the hypothesis of an overlap of Antarctica on the Beira High, which was assumed in several studies (Gaina et al., 2013, Reeves et al., 2016; Nguyen et al., 2016). As proposed by recent studies, the Beira High seems to be a microcontinent (König and Jokat, 2010; Mahanjane, 2012; Mueller et al., 2016, 2017; Senkans et al., 2019), stretched and intruded at the beginning of the Gondwana rifting. This scenario supports the reconstruction model proposed by Thompson (2017). During a first rifting stage and until 166 Ma, the continental crust was thinned in the Zambezi depression, on the African side. Then, this continental rift was aborted and

followed by a jump to the SE of the Beira High around 166-164 Ma, on the Antarctic side. The breakup followed around 157 Ma, leading to the accretion of oceanic crust between the Beira High and Antarctica (Mahanjane, 2012; Mueller et al., 2019; Thompson, 2017).

5-4 Origin of rift abortion and jump south of the Beira High

The mechanisms causing a migration of the locus of extension remain under debate. We discussed several models concerning the processes responsible for the formation of the Beira High.

- Following a long phase of tectonic quiescence, the strength of a thinned lithosphere may be higher than elsewhere. In this case, the rift axis may jump to a weaker location. This hypothesis is less likely in our study area because of the very short period of tectonic quiescence (5 Myr) of the Zambezi depression. Indeed, Naliboff and Buiter (2015) postulate a time span of 20 to 60 Myr, although this time interval highly depends on the mechanical and thermal properties of the lithosphere. Van Wijk and Cloetingh (2002) also showed in their modelling results that the time gap between the succession of rifting is of the same order, and comparable to the time gap observed in the mid-Norwegian rift zones. .
- A slow extension is another way to harden the lithosphere through concomitant cooling and thus, to abandon the rift axis (Kusznir and Parks, 1987; Naliboff and Buiter, 2015). This hypothesis can be assumed in the Zambezi depression, as the main half-extension rates are lower than 10 mm/yr. When rifting is not magma-assisted anymore, the force required to continue extension increases (Buck, 2004), and it is easier for the spreading ridge to jump to an adjacent weaker continental domain (Abera et al., 2016). However, the magmatic activity affecting the Mozambique margin is significant between 183 Ma and 157 Ma (Fig. 2), given the SDRs and lava flows on the Beira High flanks. A decrease of magmatism is only observed after 157 Ma (Mueller et al., 2017). Therefore, this hypothesis cannot explain the southward jump.
- The relocation of the rift south of Beira High may coincide with a change in plate divergence direction (Mueller et al., 2019). The initial WNW-ESE separation between Africa and Antarctica

led to a first extension phase in the Zambezi depression. However, a change of Antarctica plate motion to the south may be responsible for the jump of the spreading center south of Beira High (Mahanjane, 2012). The last statement can be favored regarding the plate reconstructions proposed in recent studies.

Further studies might provide arguments to ascertain the processes responsible for the abortion of the rifting in the Zambezi depression and the jump of the spreading center south of the Beira High.

6- CONCLUSIONS

Five scenarios with varying crustal nature and magmatic supply were tested by comparing the modelled thermal field with temperatures of available wells. Three scenarios assumed a continental origin for the Beira High, with the Zambezi depression being a thinned continental crust (model 1a), a continental crust with magmatic underplate (1b) or with magmatic along the whole margin (1c). In these scenarios, the rifting is localized north of the Beira High in a first stage. Then, extension jumps southward and leads to breakup and oceanic accretion around 157 Ma. In the third scenario, the first rifting phase leads to oceanic accretion around 164 Ma, concomitantly with the northern Angoche margin. Eventually, this oceanic accretion is aborted and relocated south of the Beira High, which remains continental. Finally, in the last scenario, rifting leads to the development of an oceanic crust in the Zambezi depression and the Beira High.

Our results show that the thermal data best fit the scenarios implying a continental origin for both, the Beira High and the Zambezi depression. In the context of a volcanic-rich margin, and given the magnetic data, the presence of a magmatic underplate is likely, but the amount of magmatic supply involved remains unknown. The Beira High seems to be a continental remnant isolated from the African margin during the first steps of the Gondwana rifting. The processes leading to the aborted rift in the Zambezi depression and the jump of the extension southward are not clear. Several hypotheses related to the structural inheritance, to the rheological evolution of the crust or to the geodynamical context can be

invoked. Despite a few limitations, the kinematic modelling used in this study demonstrates the impact of deformation and crustal nature on the thermal history. Quantitative modeling, calibrated to geological and geophysical data, allows us to propose a thermal evolution along the Mozambique volcanic-rich margin during its deformation history. Data related to the Antarctic conjugate margin may greatly improve calibration and thus will give more insights into the rifting process.

References

Abera, R., Van Wijk, J., & Axen, G. (2016). Formation of continental fragments: The Tamayo Bank, Gulf of California, Mexico. Geology, 44(8), 595-598.

Allen, P. A., & Allen, J. R. (2013). Basin analysis: Principles and application to petroleum play assessment. John Wiley & Sons.

Andrés-Martínez, M., Pérez-Gussinyé, M., Armitage, J. J., & Morgan, J. P. (2019). Thermomechanical implications of sediment transport for the architecture and evolution of continental rifts and margins, Tectonics, 38, 641–665.

Baby, G. (2017). Mouvements verticaux des marges passives d'Afrique australe depuis 130 Ma, étude couplée: stratigraphie de bassin: analyse des formes du relief (Doctoral dissertation).

Bauer, K., Neben, S., Schreckenberger, B., Emmermann, R., Hinz, K., Fechner, N., Gohl, K., Schulze, A., Trumbull, R.B., & Weber, K. (2000). Deep structure of the Namibia continental margin as derived from integrated geophysical studies. Journal of Geophysical Research: Solid Earth, 105(B11), 25829-25853.

Bénard, F., Callot, J. P., Vially, R., Schmitz, J., Roest, W., Patriat, M., Loubrieu B., Team, T. E. (2010). The Kerguelen plateau: Records from a long-living/composite microcontinent. Marine and Petroleum Geology, 27(3), 633-649.

Bingen, B., Jacobs, J., Viola, G., Henderson, I. H. C., Skår, Ø., Boyd, R., Thomas, R.J., & Daudi, E. X. F. (2009). Geochronology of the Precambrian crust in the Mozambique belt in NE Mozambique, and implications for Gondwana assembly. Precambrian Research, 170(3-4), 231-255.

Bown, J. W., & White, R. S. (1995). Effect of finite extension rate on melt generation at rifted continental margins. Journal of Geophysical Research: Solid Earth, 100(B9), 18011-18029.

Braun, J., & Yamato, P. (2010). Structural evolution of a three-dimensional, finite-width crustal wedge. Tectonophysics, 484(1-4), 181-192.

Bristow, J. W., & Saggerson, E. P. (1983). A review of Karoo vulcanicity in southern Africa. Bulletin volcanologique, 46(2), 135-159.

Brune, S., Heine, C., Clift, P.D., Pérez-Gussinyé, M., (2017). Rifted margin architecture and crustal rheology: Reviewing Iberia-Newfoundland, Central South Atlantic, and South China Sea. Marine and Petroleum Geology.

Buck, W. R., & Karner, G. D. (2004). Consequences of asthenospheric variability on continental rifting. Rheology and deformation of the lithosphere at continental margins, 62, 1-30.

Burke, K., & Dewey, J. F. (1973). Plume-generated triple junctions: key indicators in applying plate tectonics to old rocks. The Journal of Geology, 81(4), 406-433.

Burov, E., & Cloetingh, S. A. P. L. (1997). Erosion and rift dynamics: new thermomechanical aspects of post-rift evolution of extensional basins. Earth and Planetary Science Letters, 150(1-2), 7-26.

Callies, M., Filleaudeau, P. Y., Dubille, M., & Lorant, F. (2017). How to predict thermal stress in hyper extended margins application of a new lithospheric model on the Iberia Margin. AAPG Bulletin. Volume 20, 170-712.
Castelino, J. A., Reichert, C., Klingelhoefer, F., Aslanian, D., & Jokat, W. (2015). Mesozoic and Early Cenozoic sediment influx and morphology of the Mozambique Basin. Marine and Petroleum Geology, 66, 890-905.
Catuneanu, O., Wopfner, H., Eriksson, P. G., Cairncross, B., Rubidge, B. S., Smith, R. M. H., & Hancox, P. J. (2005). The Karoo basins of south-central Africa. Journal of African Earth Sciences, 43(1-3), 211-253.
Clark, S. R. (2018). Uncertainty in the breakup, spreading history, and velocity variations of Gondwana. Gondwana Research, 53, 189-196.
Cox, K. G. (1992). Karoo igneous activity, and the early stages of the break-up of Gondwanaland. Geological Society, London, Special Publications, 68(1), 137-148.
Crosby, A.G., White, N.J., Edwards, G.R.H., & Shillington, D. J. (2008). Evolution of the Newfoundland–Iberia conjugate rifted margins. Earth Planet. Sci. Lett.. Volume 273(1-2), 214-226.
Davis, J. K., Lawver, L. A., Norton, I. O., & Gahagan, L. M. (2016). New Somali Basin magnetic anomalies and a plate model for the early Indian Ocean. Gondwana research, 34, 16-28.
Dias Svartman, A. E., Hayman, N. W., Lavier L.L., (2016). Thinning factor distributions viewed through numerical models of continental extension. Tectonics. Volume 35, 3050 – 3069.
Duncan, R. A., Hooper, P. R., Rehacek, J., Marsh, J., & Duncan, A. R. (1997). The timing and duration of the Karoo igneous event, southern Gondwana. Journal of Geophysical Research: Solid Earth, 102(B8), 18127-18138.
Eagles, G., & König, M. (2008). A model of plate kinematics in Gondwana breakup. Geophysical Journal International. Volume 173(2), 703-717.
Emmel, B., Kumar, R., Ueda, K., Jacobs, J., Daszinnies, M. C., Thomas, R. J., & Matola, R. (2011). Thermochronological history of an orogen-passive margin system: An example from northern Mozambique. Tectonics, 30(2).
Encarnación, J., Fleming, T. H., Elliot, D. H., & Eales, H. V. (1996). Synchronous emplacement of Ferrar and Karoo dolerites and the early breakup of Gondwana. Geology, 24(6), 535-538.
Fitch, F. J., & Miller, J. A. (1984). Dating Karoo igneous rocks by the conventional K-Ar and 40 Ar/39 Ar age spectrum methods.
Flores, G. (1964). On the age of the Lupata rocks, lower Zambezi River, Mozambique. South African Journal of Geology, 67(Transactions 1964), 111-118.
Franke, D., Neben, S., Ladage, S., Schreckenberger, B., & Hinz, K. (2007). Margin segmentation and volcano-tectonic architecture along the volcanic margin off Argentina/Uruguay, South Atlantic. Marine Geology, 244(1-4), 46-67.
Franke, D., Ladage, S., Schnabel, M., Schreckenberger, B., Reichert, C., Hinz, K.,Paterlini, M., De Abelleyra, J., & Siciliano, M. (2010). Birth of a volcanic margin off Argentina, South Atlantic. Geochemistry, Geophysics, Geosystems, 11(2).
Gaina, C., Muller, R. D., Brown, B. J., & Ishihara, T. (2003). Microcontinent formation around Australia. Special papers-geological society of America, 405-416.
Gaina, C., Torsvik, T. H., van Hinsbergen, D. J., Medvedev, S., Werner, S. C., & Labails, C. (2013). The African Plate: A history of oceanic crust accretion and subduction since the Jurassic. Tectonophysics, 604, 4-25.
Gaina, C., Van Hinsbergen, D. J., & Spakman, W. (2015). Tectonic interactions between India and Arabia since the Jurassic reconstructed from marine geophysics, ophiolite geology, and seismic tomography. Tectonics, 34(5), 875-906.
Garner, P. (1996). Continental flood basalts indicate a pre-Mesozoic Flood/post-Flood boundary. Creation Ex Nihilo Technical Journal, 10(1), 114-126.
Geoffroy, L. (2005). Volcanic passive margins. Comptes Rendus Geoscience, 337(16), 1395-1408.

Geoffroy, L., Burov, E. B., & Werner, P. (2015). Volcanic passive margins: another way to break up continents. Scientific Reports, 5, 14828.
Gernigon, L., Blischke, A., Nasuti, A., & Sand, M. (2015). Conjugate volcanic rifted margins, seafloor spreading, and microcontinent: Insights from new high-resolution aeromagnetic surveys in the Norway Basin. Tectonics, 34(5), 907-933.
Glerum, A., Brune, S., Stamps, D. S., & Strecker, M. R. (2020). Victoria continental microplate dynamics controlled by the lithospheric strength distribution of the East African Rift. Nature Communications, 11(1), 2881. https://doi.org/10.1038/s41467-020-16176-x
Hasterok, D., Gard, M., & Webb, J. (2018). On the radiogenic heat production of metamorphic, igneous, and sedimentary rocks. Geoscience Frontiers, 9(6), 1777-1794.
Hastie, A. R., Fitton, J. G., Kerr, A. C., McDonald, I., Schwindrofska, A., & Hoernle, K. (2016). The composition of mantle plumes and the deep Earth. Earth and Planetary Science Letters, 444, 13-25.
Huismans, R., Beaumont, C., (2014). Rifted continental margins: the case for depth-dependent extension. Earth Planet. Sci. Lett.. Volume 407, 148 – 162.
Jacobs, J., Klemd, R., Fanning, C. M., Bauer, W., & Colombo, F. (2003). Extensional collapse of the late Neoproterozoic-early Palaeozoic East African-Antarctic Orogen in central Dronning Maud Land, East Antarctica. Geological Society, London, Special Publications, 206(1), 271-287.
Jacobs, J., Pisarevsky, S., Thomas, R. J., & Becker, T. (2008). The Kalahari Craton during the assembly and dispersal of Rodinia. Precambrian Research, 160(1-2), 142-158.
Jeanniot, L., Kusznir, N., Mohn, G., Manatschal, G., & Cowie, L. (2016). Constraining lithosphere deformation modes during continental breakup for the Iberia–Newfoundland conjugate rifted margins. Tectonophysics. Volume 680, 28-49.
Jokat, W., Boebel, T., König, M., & Meyer, U. (2003). Timing and geometry of early Gondwana breakup. Volume 108(B9).
Jokat, W. (2014). The expedition of the research vessel" Sonne" to the Mozambique Basin in 2014 (SO230). Berichte zur Polar-und Meeresforschung= Reports on polar and marine research, 676.
Jourdan, F., Féraud, G., Bertrand, H., Kampunzu, A. B., Tshoso, G., Watkeys, M. K., & Le Gall, B. (2005). Karoo large igneous province: Brevity, origin, and relation to mass extinction questioned by new 40Ar/39Ar age data. Geology, 33(9), 745-748.
Jourdan, F., Bertrand, H., Schärer, U., Blichert-Toft, J., Féraud, G., & Kampunzu, A. B. (2007). Major and trace element and Sr, Nd, Hf, and Pb isotope compositions of the Karoo large igneous province, Botswana–Zimbabwe: lithosphere vs mantle plume contribution. Journal of Petrology, 48(6), 1043-1077.
Jourdan, F., Féraud, G., Bertrand, H., Watkeys, M. K., & Renne, A. P. (2008). The 40Ar/39Ar ages of the sill complex of the Karoo large igneous province: Implications for the Pliensbachian-Toarcian climate change. Geochemistry, Geophysics, Geosystems, 9(6).
Katz, R. F., Spiegelman, M., & Langmuir, C. H. (2003). A new parameterization of hydrous mantle melting. Geochemistry, Geophysics, Geosystems, 4(9).
Klausen, M. B. (2009). The Lebombo monocline and associated feeder dyke swarm: Diagnostic of a successful and highly volcanic rifted margin?. Tectonophysics. Volume 468(1-4), 42-62.
Klimke, J., Franke, D., Estevão, S. M., & Leitchenkov, G. (2018). Tie points for Gondwana reconstructions from a structural interpretation of the Mozambique Basin, East Africa and the Riiser-Larsen Sea, Antarctica. Solid Earth, 9(1), 25.
König, M., & Jokat, W. (2006). The Mesozoic breakup of the Weddell Sea. Journal of Geophysical Research: Solid Earth, 111(B12).
König, M., & Jokat, W. (2010). Advanced insights into magmatism and volcanism of the Mozambique Ridge and Mozambique Basin in the view of new potential field data. Geophysical Journal International. Volume 180(1), 158-180.
Kelemen, P. B., & Holbrook, W. S. (1995). Origin of thick, high-velocity igneous crust along the US East Coast Margin. Journal of Geophysical Research: Solid Earth, 100(B6), 10077-10094.

Key, R. M., Smith, R. A., Smelror, M., Sæther, O. M., Thorsnes, T., Powell, J. H., Njange, F., & Zandamela, E. B. (2008). Revised lithostratigraphy of the Mesozoic-Cenozoic succession of the onshore Rovuma Basin, northern coastal Mozambique. South African Journal of Geology, 111(1), 89-108.

Kovacs, L. C., Morris, P., Brozena, J., & Tikku, A. (2002). Seafloor spreading in the Weddell Sea from magnetic and gravity data. Tectonophysics, 347(1-3), 43-64.

Kumar, P., & Kawakatsu, H. (2011). Imaging the seismic lithosphere-asthenosphere boundary of the oceanic plate. Geochemistry, Geophysics, Geosystems, 12(1).

Kusznir, N. J., & Park, R. G. (1987). The extensional strength of the continental lithosphere: its dependence on geothermal gradient, and crustal composition and thickness. Geological Society, London, Special Publications, 28(1), 35-52.

Kusznir, N. J., & Karner, G. D. (2007). Continental lithospheric thinning and breakup in response to upwelling divergent mantle flow: application to the Woodlark, Newfoundland and Iberia margins. Geological Society, London, Special Publications. Volume 282(1), 389-419.

Leinweber, V. T., & Jokat, W. (2012). The Jurassic history of the Africa–Antarctica corridor—new constraints from magnetic data on the conjugate continental margins. Tectonophysics. Volume 530, 87-101.

Leinweber, V. T., Klingelhoefer, F., Neben, S., Reichert, C., Aslanian, D., Matias, L., Heyde, I., Schreckenberger, B., & Jokat, W. (2013). The crustal structure of the Central Mozambique continental margin—Wide-angle seismic, gravity and magnetic study in the Mozambique Channel, Eastern Africa. Tectonophysics, 599, 170-196.

Leitchenkov, G., Guseva, J., Gandyukhin, V., Grikurov, G., Kristoffersen, Y., Sand, M., Golynsky, A., & Aleshkova, N. (2008). Crustal structure and tectonic provinces of the Riiser-Larsen Sea area (East Antarctica): results of geophysical studies. Marine Geophysical Researches, 29(2), 135-158.

Le Gal, V., Lucazeau, F., Cannat, M., Poort, J., Monnin, C., Battani, A., Fontaine, F., Goutorbe., B., Rolandone., F., Piedale, A., Hipólito, A., & Blanc-Valleron, M. M. (2018). Heat flow, morphology, pore fluids and hydrothermal circulation in a typical Mid-Atlantic Ridge flank near Oceanographer Fracture Zone. Earth and Planetary Science Letters, 482, 423-433.

Le Pichon, X., & Heirtzler, J. R. (1968). Magnetic anomalies in the Indian Ocean and sea-floor spreading. Journal of Geophysical Research, 73(6), 2101-2117.

Leroy, S., Lucazeau, F., d'Acremont, E., Watremez, L., Autin, J., Rouzo, S., Bllahsen, N., Tiberi, C., Ebinger, C., Beslier, M.-O., Perrot, J., Razin, P., Rolandone, F., Sloan, H., Stuart, G., Al Lazki, A., Al-Toubi, K., Bache, F., Bonneville, A., Goutorbe, B., Huchon, P., Unternehr, P., & Khanbari, K. (2010). Contrasted styles of rifting in the eastern Gulf of Aden: A combined wide-angle, multichannel seismic, and heat flow survey. Geochemistry, Geophysics, Geosystems, 11(7).

Lucazeau, F., Leroy, S., Rolandone, F., d'Acremont, E., Watremez, L., Bonneville, A., Goutorbe, B., & Düsünur, D. (2010). Heat-flow and hydrothermal circulation at the ocean–continent transition of the eastern Gulf of Aden. Earth and Planetary Science Letters, 295(3-4), 554-570.

Mahanjane, E. S. (2012). A geotectonic history of the northern Mozambique Basin including the Beira High–a contribution for the understanding of its development. Marine and Petroleum Geology, 36(1), 1-12.

Mahanjane, E. S. (2014). The Davie Fracture Zone and adjacent basins in the offshore Mozambique Margin–A new insights for the hydrocarbon potential. Marine and Petroleum Geology, 57, 561-571.

Mahanjane, E. S., Franke, D., Lutz, R., Winsemann, J., Ehrhardt, A., Berglar, K., & Reichert, C. (2014). Maturity and petroleum systems modelling in the offshore Zambezi Delta depression and Angoche Basin, northern Mozambique. Journal of Petroleum Geology, 37(4), 329-348.

Martin, A. K., & Hartnady, C. J. H. (1986). Plate tectonic development of the South West Indian Ocean: A revised reconstruction of East Antarctica and Africa. Journal of Geophysical Research: Solid Earth, 91(B5), 4767-4786.

Martin, A. K. (2007). Gondwana breakup via double-saloon-door rifting and seafloor spreading in a back arc basin during subduction rollback. Tectonophysics, 445(3-4), 245-272.

McKenzie, D., & Bickle, M. J. (1988). The volume and composition of melt generated by extension of the lithosphere. Journal of petrology, 29(3), 625-679.
McElhinny, M. W. (1970). Formation of the Indian Ocean. Nature, 228(5275), 977.
Menzies, M. A., Klemperer, S. L., Ebinger, C. J., & Baker, J. (2002). Characteristics of volcanic rifted margins. Special Papers-Geological Society of America, 1-14.
Meyer, R., Van Wijk, J., & Gernigon, L. (2007). The North Atlantic Igneous Province: A review of models for its formation. Geological Society of America Special Papers, 430, 525-552.
Milesi, J. P., Commission de la carte géologique du monde. Sous-commission de la carte tectonique du monde, de Lamotte, D. F., De Kock, G. S., & Unesco. (2010). Carte tectonique de l'Afrique: Tectonic Map of Africa. CCGM/UNESCO.
Mueller, C. O., Jokat, W., & Schreckenberger, B. (2016). The crustal structure of Beira High, central Mozambique—Combined investigation of wide-angle seismic and potential field data. Tectonophysics. Volume 683, 233-254.
Mueller, C. O., & Jokat, W. (2017). Geophysical evidence for the crustal variation and distribution of magmatism along the central coast of Mozambique. Tectonophysics. Volume 712, 684-703.
Mueller, C. O., & Jokat, W. (2019). The initial Gondwana break-up: A synthesis based on new potential field data of the Africa-Antarctica Corridor. Tectonophysics, 750, 301-328.
Müller, R. D., Gaina, C., Roest, W. R., & Hansen, D. L. (2001). A recipe for microcontinent formation. Geology, 29(3), 203-206.
Nairn, A. E., Lerche, I., & Iliffe, J. E. (1991). Geology, basin analysis, and hydrocarbon potential of Mozambique and the Mozambique Channel. Earth-Science Reviews, 30(1-2), 81-123.
Naliboff, J., & Buiter, S. J. (2015). Rift reactivation and migration during multiphase extension. Earth and Planetary Science Letters, 421, 58-67.
Nemčok, M. (2016). Rifts and passive margins: Structural architecture, thermal regimes, and petroleum systems. Cambridge University Press.
Nguyen, L. C., S. A. Hall, D. E. Bird, and P. J. Ball (2016), Reconstruction of the East Africa and Antarctica continental margins. J. Geophys. Res. Solid Earth. Volume 21, 4156–4179.
Norton, I. O., & Sclater, J. G. (1979). A model for the evolution of the Indian Ocean and the breakup of Gondwanaland. Journal of Geophysical Research: Solid Earth, 84(B12), 6803-6830.
Pasquale, V., Verdoya, M., & Chiozzi, P. (2014). Heat Conduction and Thermal Parameters. In Geothermics (pp. 15-52). Springer, Cham.
Phethean, J. J., Kalnins, L. M., van Hunen, J., Biffi, P. G., Davies, R. J., & McCaffrey, K. J. (2016). Madagascar's escape from Africa: A high-resolution plate reconstruction for the Western Somali Basin and implications for supercontinent dispersal. Geochemistry, Geophysics, Geosystems, 17(12), 5036-5055.
Planke, S., Symonds, P. A., Alvestad, E., & Skogseid, J. (2000). Seismic volcanostratigraphy of large-volume basaltic extrusive complexes on rifted margins. Journal of Geophysical Research: Solid Earth, 105(B8), 19335-19351.
Ponte, J. P. (2018). La marge africaine du canal du Mozambique, le système turbiditique du Zambèze: une approche «Source to Sink» au Méso–Cénozoïque (Doctoral dissertation, Université Rennes 1).
Reeves, C. (2000). The geophysical mapping of Mesozoic dyke swarms in southern Africa and their origin in the disruption of Gondwana. Journal of African earth sciences, 30(3), 499-513.
Reeves, C. V., Sahu, B. K., & De Wit, M. (2002). A re-examination of the paleo-position of Africa's eastern neighbours in Gondwana. Journal of African Earth Sciences, 34(3-4), 101-108.
Reeves, C. V., Teasdale, J. P., & Mahanjane, E. S. (2016). Insight into the Eastern Margin of Africa from a new tectonic model of the Indian Ocean. Geological Society, London, Special Publications, 431(1), 299-322.
Riedel, S., Jacobs, J., & Jokat, W. (2013). Interpretation of new regional aeromagnetic data over Dronning Maud Land (East Antarctica). Tectonophysics, 585, 161-171.

Riley, T. R., Leat, P. T., Kelley, S. P., Millar, I. L., & Thirlwall, M. F. (2003). Thinning of the Antarctic Peninsula lithosphere through the Mesozoic: evidence from Middle Jurassic basaltic lavas. Lithos, 67(3-4), 163-179.

Röhl, U., Westerhold, T., Bralower, T. J., & Zachos, J. C. (2007). On the duration of the Paleocene-Eocene thermal maximum (PETM). Geochemistry, Geophysics, Geosystems, 8(12).

Senkans, A., Leroy, S., d'Acremont, E., Castilla, R., & Despinois, F. (2019). Polyphase rifting and break-up of the central Mozambique margin. Marine and Petroleum Geology, 100, 412-433.

Segev, A. (2002). Flood basalts, continental breakup and the dispersal of Gondwana: evidence for periodic migration of upwelling mantle flows (plumes). EGU Stephan Mueller Special Publication Series, 2, 171-191.

Segoufin, J. (1978). Anomalies magnétiques mésozoïques dans le Bassin de Mozambique.

Seton, M., Müller, R. D., Zahirovic, S., Gaina, C., Torsvik, T., Shephard, G., Talsma, A., Gurnis, M., Turner, M., Maus, S., & Chandler, M. (2012). Global continental and ocean basin reconstructions since 200 Ma. Earth-Science Reviews, 113(3-4), 212-270.

Simpson, E. S. W., Sclater, J. G., Parsons, B., Norton, I., & Meinke, L. (1979). Mesozoic magnetic lineations in the Mozambique Basin. Earth and Planetary Science Letters, 43(2), 260-264.

Smith, A. G., & Hallam, A. (1970). The fit of the southern continents. Nature, 225(5228), 139-144.

Spadini, G., Cloetingh, S., & Bertotti, G. (1995). Thermo-mechanical modeling of the Tyrrhenian Sea: Lithospheric necking and kinematics of rifting. Tectonics, 14(3), 629-644.

Spadini, G., Robinson, A. G., & Cloetingh, S. A. P. L. (1997). Thermo-mechanical modelling of the Black Sea basin formation, subsidence and sedimentation. AAPG memoir, 68, 19-38.

Storey, B. C. (1995). The role of mantle plumes in continental breakup: case histories from Gondwanaland. Nature, 377(6547), 301.

Svensen, H., Corfu, F., Polteau, S., Hammer, Ø., & Planke, S. (2012). Rapid magma emplacement in the Karoo large igneous province. Earth and Planetary Science Letters, 325, 1-9.

Thompson, J. (2017). The Opening of the Indian Ocean: What is the Impact on the East African, Madagascar and Antarctic Margins, and what are the Origins of the Aseismic Ridges? (Doctoral dissertation)

Torsvik, T. H., Müller, R. D., Van der Voo, R., Steinberger, B., & Gaina, C. (2008). Global plate motion frames: toward a unified model. Reviews of geophysics, 46(3).

Torsvik, T. H., Amundsen, H., Hartz, E. H., Corfu, F., Kusznir, N., Gaina, C., Doubrovine, P. V., Steinberger, B., Ashwal, L. D. Jamtveit, B. (2013). A Precambrian microcontinent in the Indian Ocean. Nature Geoscience, 6(3), 223-227.

Van den Broek, J. M., & Gaina, C. Microcontinents and continental fragments associated with subduction systems. Tectonics, e2020TC006063.

Van den Broek, J. M., Magni, V., Gaina, C., & Buiter, S. J. H. (2020). The formation of continental fragments in subduction settings: the importance of structural inheritance and subduction system dynamics. Journal of Geophysical Research: Solid Earth, 125(1), e2019JB018370.

Van Wijk, J. W., and S. A. P. L. Cloetingh. "Basin migration caused by slow lithospheric extension." Earth and Planetary Science Letters 198.3-4 (2002): 275-288.

Watkeys, M. K. (2002). Development of the Lebombo rifted volcanic margin of southeast Africa. Special papers-geological society of America, 27-46.

Watts, A. B. (2001). Gravity anomalies, flexure and crustal structure at the Mozambique rifted margin. Marine and Petroleum Geology, 18(4), 445-455.

Wernicke, B. (1981) Low-angle normal faults in the Basin and Range province: Nappe tectonics in an extending orogen: Nature, v. 291, p. 645-648.

White, R. S., Smith, L. K., Roberts, A. W., Christie, P. A. F., & Kusznir, N. J. (2008). Lower-crustal intrusion on the North Atlantic continental margin. Nature, 452(7186), 460.

Will, T. M., & Frimmel, H. E. (2018). Where does a continent prefer to break up? Some lessons from the South Atlantic margins. Gondwana Research, 53, 9-19.

Model 1a

Events	1	2	3	4	5	6	7	8	9	10	11
Start Event (Ma)	183	178	173	168	166	164	161	157	151	140	0
End Event (Ma)	178	173	168	166	164	161	157	151	140	0	0
Event Duration (Myr)	5	5	5	2	2	3	4	6	11	140	0
Cumulative Model Time (Myr)	5	10	15	17	19	22	26	32	43	183	183
Deformation Half Width (km)	150	50	50	50	65	50	40	25	25	25	0
Half Spreading Rate (km/Myr)	4.50...	6.50...	7	6	6.50...	7.50...	10	12	22	0	0
Buoyancy/UDF upwelling Rate (km/Myr)	0	7.50...	8	30	40	12	2	0	0	0	0
Buoyancy/UDF Action Depth (km)	40	40	40	35	30	25	25	25	25	25	0
Location Pure-Shear axis (km)	0	-115	-100	20	40	110	70	75	75	75	0
Migration Pure-Shear axis	0	0.40...	0	0	0	-0.4...	-0.2	0	0	0	0
Location Buoyancy axis (km)	0	-90	-90	-60	-20	20	60	75	75	75	0
Migration Buoyancy axis	0	1	3	5	5	3	3	0	0	0	0
Location Melt extraction axis (km)	0	-100	-100	-110	-50	70	70	75	75	75	0
Migration Melt extraction axis	0	0	0	0	0	0.10...	0.10...	0	0	0	0
Melt extraction width (km)	0	50	50	50	50	50	40	40	25	25	0
Melt underplated width (km)	0	0	0	0	0	0	0	0	0	0	0
Melt threshhold prior extraction (%)	0	0	0	0	0	0	0	0	0	0	0
Melt retained in mantle (%)	0	0	0	60	100	40	30	20	20	0	0
Melt being underplated (%)	0	0	0	0	0	0	0	0	0	0	0

Model 1b

Events	1	2	3	4	5	6	7	8	9	10	11
Start Event (Ma)	183	178	173	168	166	164	161	157	151	140	0
End Event (Ma)	178	173	168	166	164	161	157	151	140	0	0
Event Duration (Myr)	5	5	5	2	2	3	4	6	11	140	0
Cumulative Model Time (Myr)	5	10	15	17	19	22	26	32	43	183	0
Deformation Half Width (km)	150	40	40	50	65	50	40	25	25	25	0
Half Spreading Rate (km/Myr)	2	7.50...	9	4.50...	10	7.50...	10	12	22	0	0
Buoyancy/UDF upwelling Rate (km/Myr)	0	25	30	35	40	12	2	0	0	0	0
Buoyancy/UDF Action Depth (km)	40	40	35	35	30	25	25	25	25	25	0
Location Pure-Shear axis (km)	0	-105	-100	30	40	110	70	75	75	75	0
Migration Pure-Shear axis	0	0.20...	0	0	0.20...	-0.4...	-0.2...	0	0	0	0
Location Buoyancy axis (km)	0	-90	-90	-40	0	20	60	75	75	75	0
Migration Buoyancy axis	0	1	2	5	6	4	3	0	0	0	0
Location Melt extraction axis (km)	0	-105	-100	90	-50	70	80	75	75	75	0
Migration Melt extraction axis	0	0	0.10...	0.10...	0	0.10...	0.10...	0	0	0	0
Melt extraction width (km)	0	50	50	50	50	50	40	40	25	25	0
Melt underplated width (km)	0	55	55	55	0	0	0	0	0	0	0
Melt threshhold prior extraction (%)	0	0	0	0	0	0	0	0	0	0	0
Melt retained in mantle (%)	0	0	0	50	100	100	30	20	20	0	0
Melt being underplated (%)	0	85	85	85	0	0	0	0	0	0	0

Model 1c

Events	1	2	3	4	5	6	7	8	9	10	11
Start Event (Ma)	183	178	172	168	166	164	161	157	151	140	0
End Event (Ma)	178	172	168	166	164	161	157	151	140	0	0
Event Duration (Myr)	5	6	4	2	2	3	4	6	11	0	0
Cumulative Model Time (Myr)	5	11	15	17	19	22	26	32	43	43	0
Deformation Half Width (km)	150	40	40	40	50	65	25	25	25	25	0
Half Spreading Rate (km/Myr)	3	9	9	5	4	6	12	15	22	0	0
Buoyancy/UDF upwelling Rate (km/Myr)	0	15	20	55	55	40	20	0	0	0	0
Buoyancy/UDF Action Depth (km)	40	40	30	30	30	30	30	25	25	25	0
Location Pure-Shear axis (km)	-10	-105	-95	10	10	-10	60	65	75	75	0
Migration Pure-Shear axis	0	0.40...	0	0	0	0.60...	-0.4...	0.50...	0	0	0
Location Buoyancy axis (km)	-10	-90	-90	-80	-40	20	55	50	75	75	0
Migration Buoyancy axis	0	0	1	3	3	2	1	1	0	0	0
Location Melt extraction axis (km)	-10	-90	-90	-30	-20	50	40	35	75	75	0
Migration Melt extraction axis	0	0	0	0.30...	0.25...	0.20...	0.60...	1	0	0	0
Melt extraction width (km)	45	45	40	20	40	40	35	35	35	35	0
Melt underplated width (km)	45	40	40	20	25	25	35	0	0	0	0
Melt threshhold prior extraction (%)	0	0	0	0	0	0	0	0	0	0	0
Melt retained in mantle (%)	0	0	0	0	0	0	0	0	0	0	0
Melt being underplated (%)	60	60	60	100	100	100	100	0	0	0	0

Model 2

Events	1	2	3	4	5	6	7	8	9	10	11
Start Event (Ma)	183	178	178	168	166	164	161	157	151	140	0
End Event (Ma)	178	172	168	166	164	161	157	151	140	0	0
Event Duration (Myr)	5	6	10	2	2	3	4	6	11	140	0
Cumulative Model Time (Myr)	5	5	15	17	19	22	26	32	43	183	183
Deformation Half Width (km)	100	10	20	50	65	50	40	25	25	25	0
Half Spreading Rate (km/Myr)	8	10	2	3	3	9	10	12	22	0	0
Buoyancy/UDF upwelling Rate (km/Myr)	0	8	20	35	40	12	2	0	0	0	0
Buoyancy/UDF Action Depth (km)	40	40	35	35	30	25	25	25	25	25	0
Location Pure-Shear axis (km)	-50	-125	-115	20	40	95	70	75	75	75	0
Migration Pure-Shear axis	-0.2...	0.50...	0.20...	0.10...	0.20...	-0.5...	-0.2...	0	0	0	0
Location Buoyancy axis (km)	0	-90	-90	-40	0	20	60	75	75	75	0
Migration Buoyancy axis	0	1	2	5	6	4	3	0	0	0	0
Location Melt extraction axis (km)	-145	-110	-105	-105	-50	70	80	75	75	75	0
Migration Melt extraction axis	0.20...	0.10...	0	0	0	0.10...	0.10...	0	0	0	0
Melt extraction width (km)	40	35	25	25	50	50	40	40	25	25	0
Melt underplated width (km)	50	40	35	25	0	0	0	0	0	0	0
Melt threshhold prior extraction (%)	0	0	0	0	0	0	0	0	0	0	0
Melt retained in mantle (%)	0	0	0	0	100	100	30	20	0	0	0
Melt being underplated (%)	0	0	0	0	0	0	0	0	0	0	0

Model 3

Events	1	2	3	4	5	6	7	8	9	10	11
Start Event (Ma)	183	178	168	163	160	157	151	140	0	0	0
End Event (Ma)	178	168	163	160	157	151	140	0	0	0	0
Event Duration (Myr)	5	12	3	3	3	6	11	140	0	0	0
Cumulative Model Time (Myr)	5	17	20	23	26	32	43	183	183	183	183
Deformation Half Width (km)	100	50	40	40	40	25	25	25	0	0	0
Half Spreading Rate (km/Myr)	6	7	12	6	6	10	22	0	0	0	0
Buoyancy/UDF upwelling Rate (km/Myr)	0	0	53	95	75	0	0	0	0	0	0
Buoyancy/UDF Action Depth (km)	40	40	25	25	25	25	25	25	0	0	0
Location Pure-Shear axis (km)	0	-50	-80	5	30	75	100	100	0	0	0
Migration Pure-Shear axis	0	0.30...	0	0	0	-0.4...	0	0	0	0	0
Location Buoyancy axis (km)	0	-25	-40	5	0	75	100	100	0	0	0
Migration Buoyancy axis	0	0	2	2	3	0	0	0	0	0	0
Location Melt extraction axis (km)	0	-35	-80	-20	10	60	100	100	0	0	0
Migration Melt extraction axis	0	0	1	1.60...	2	0.05...	0	0	0	0	0
Melt extraction width (km)	0	65	50	35	35	40	25	25	0	0	0
Melt underplated width (km)	0	0	0	0	0	0	0	0	0	0	0
Melt threshhold prior extraction (%)	0	0	0	0	0	0	0	0	0	0	0
Melt retained in mantle (%)	0	0	0	0	0	0	0	0	0	0	0
Melt being underplated (%)	0	0	0	0	0	50	50	0	0	0	0

Sediments parameters

Events	1	2	3	4	5	6	7
Start event (Ma)	183	167	154	142	129	66	23
End event (Ma)	167	154	142	129	66	23	0
Event duration (Myr)	16	13	12	13	63	43	23
Cumulative model time	16	29	41	54	117	160	183
Global sedimentation rate (km/Myr)	0.10...	0.10...	0.04...	0.02...	0.06...	0.07...	0.29...
Global sedimentation depth (m)	10	10	500	1000	1500	1500	1500
Coastal LEFT sed rate (km/Myr)	0	0.03...	0.04...	0.05...	0.09...	0.10...	0.56...
Coastal LEFT length (km)	0	200	300	300	150	150	150
Coastal RIGHT sed rate (km/Myr)	0	0.03...	0.03...	0.04...	0.03...	0.02...	0.02...
Coastal RIGHT length (km)	0	100	100	100	100	100	100
Erosion rate (%/timestep)	0	0	0	0	0	0	0
Index layer	0	0	0	0	0	0	0

Appendix A: Table of calibration for model 1a, 1b, 1c, 2 and 3. The calibration requires the setting of deformation events of finite duration. Each model has its own calibration parameters calibrated to match the crustal architecture but they share the same sediment deposition history. Model 0 shown in appendix B follows the same deformation history as model 1a, except with no active upwelling rate (no buoyancy) at any time of the rifting.

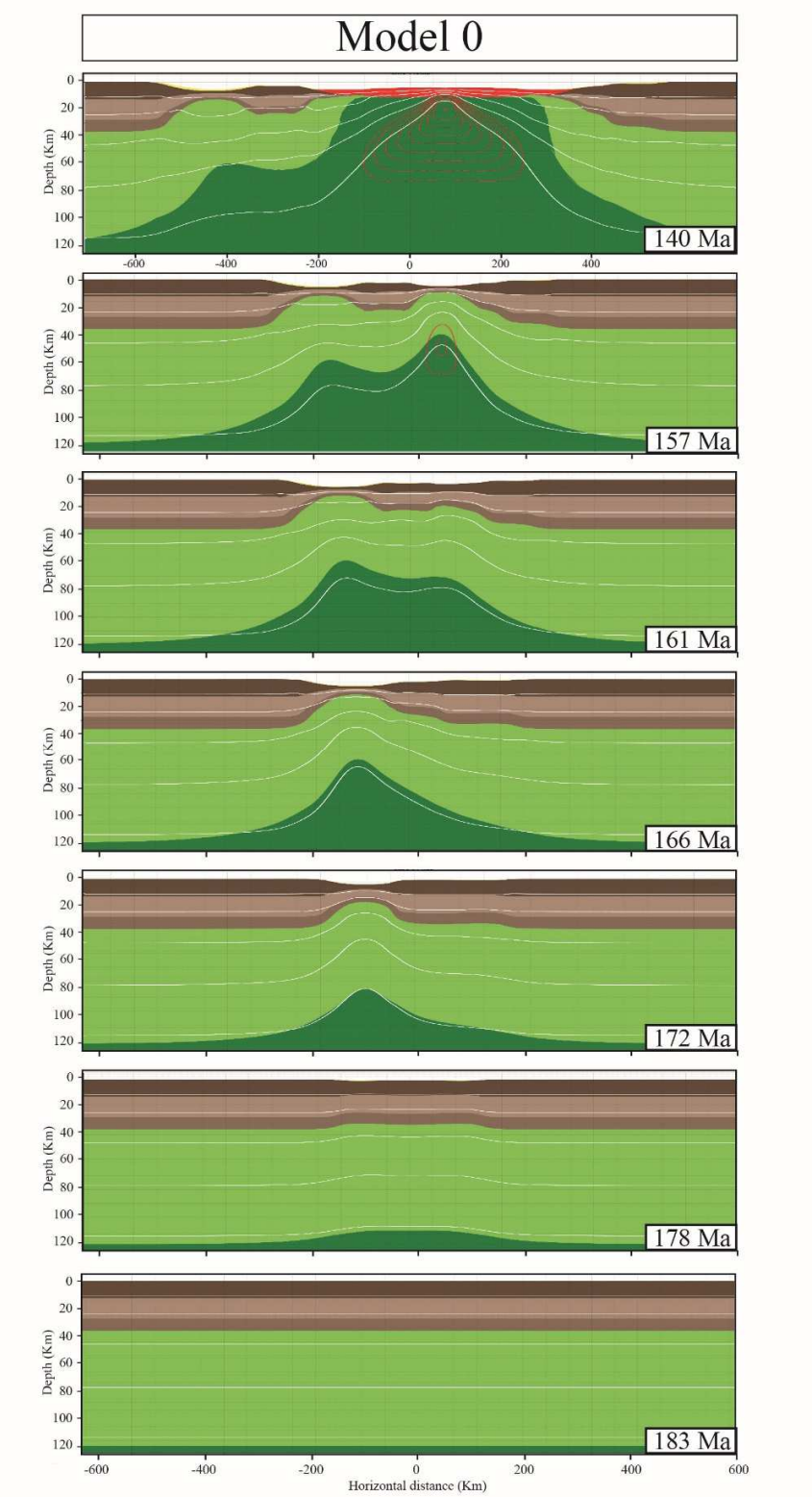

Appendix B: Evolution of the lithosphere deformation of model 0. Model 0 follows the same deformation history as model 1a, except with no active upwelling rate (no buoyancy) at any time of the rifting.

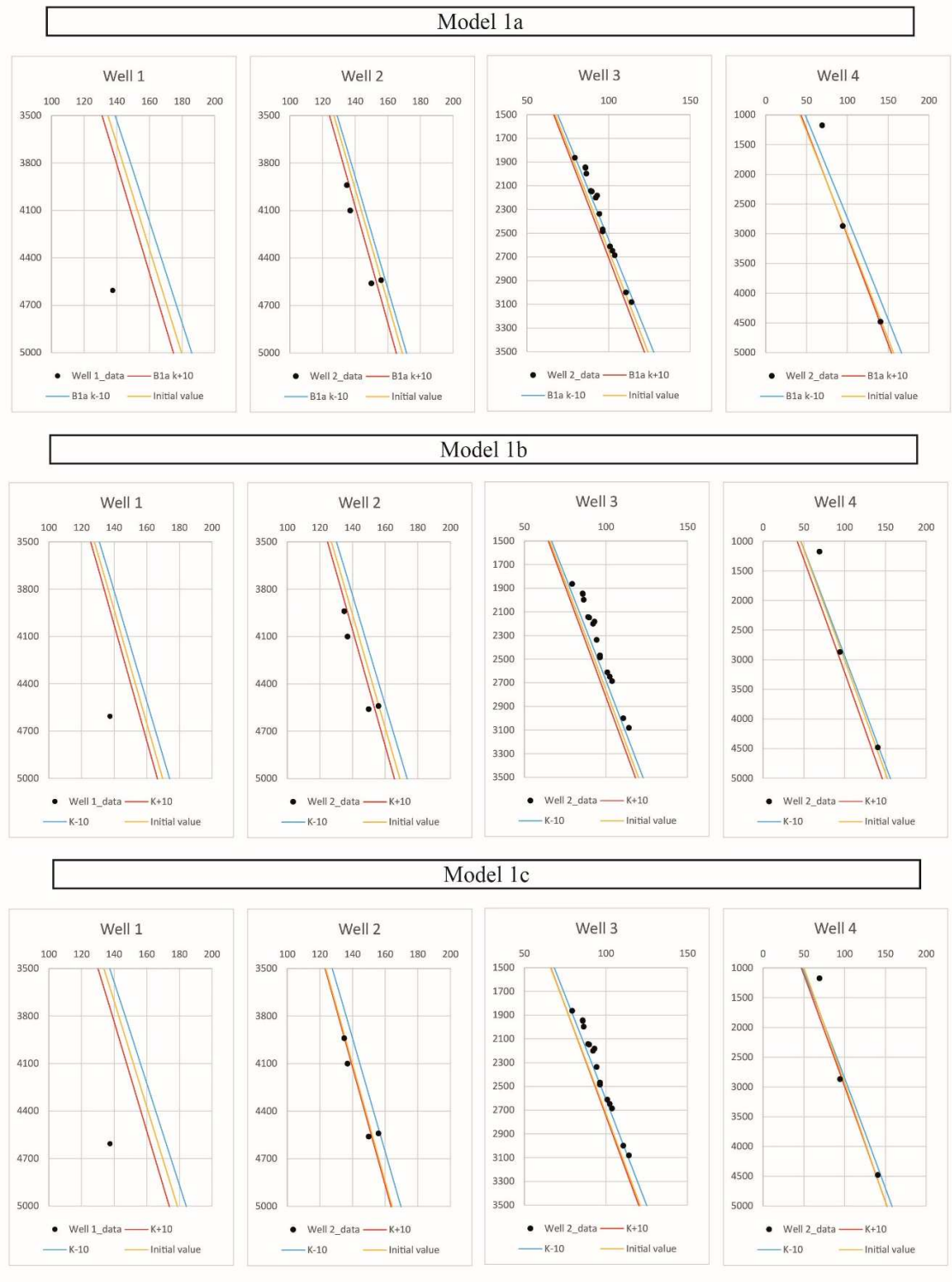

Appendix C1: We tested the sensitivity of varied thermal conductivity on model 1a, 1b and 1c. We performed a 10% variation test for all the layers. In orange are the reference thermal conductivity as stated in table 1. In red and blue are the sensitivity test of +10% and -10% thermal conductivity, respectively.

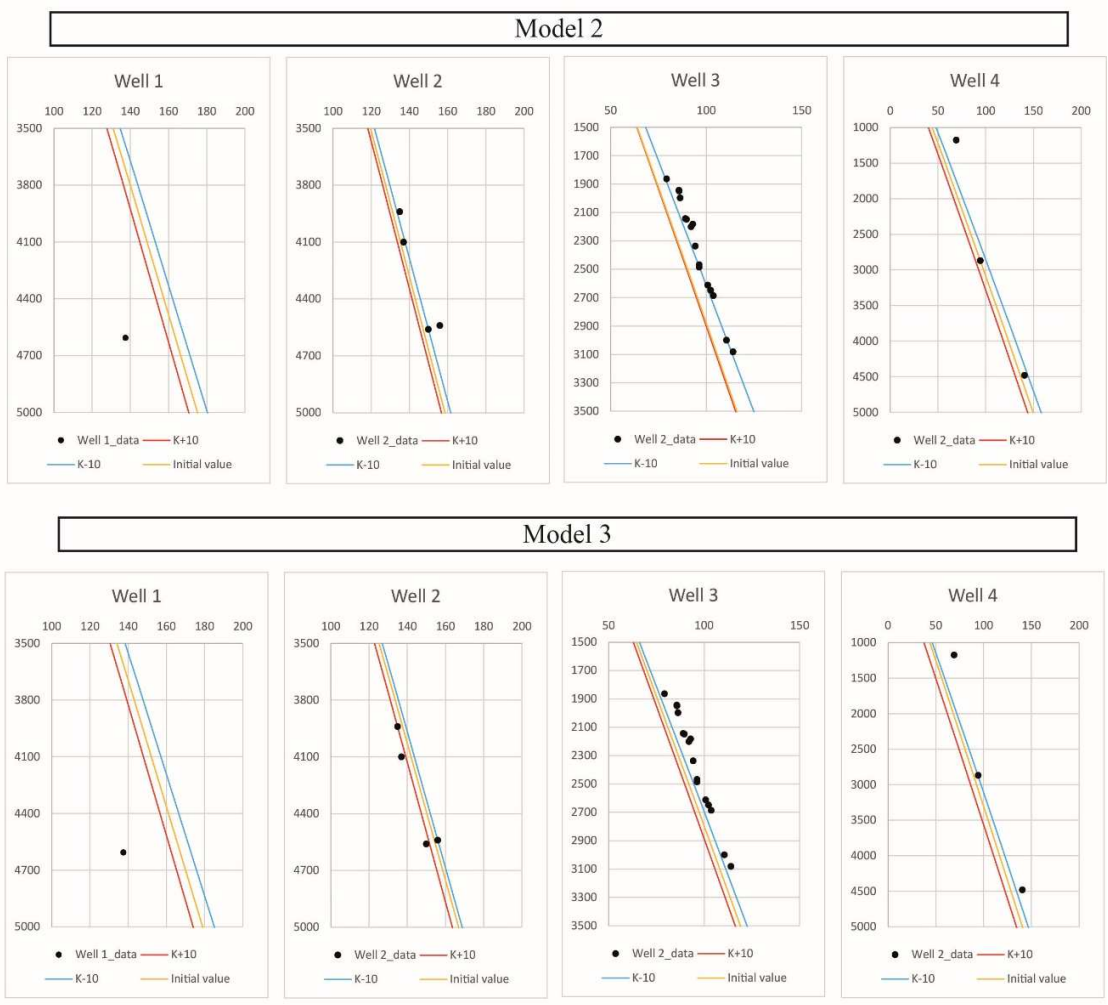

Appendix C2: We tested the sensitivity of varied thermal conductivity on model 2 and 3. We performed a 10% variation test for all the layers. In orange are the reference thermal conductivity as stated in table 1. In red and blue are the sensitivity test of +10% and -10% thermal conductivity, respectively.

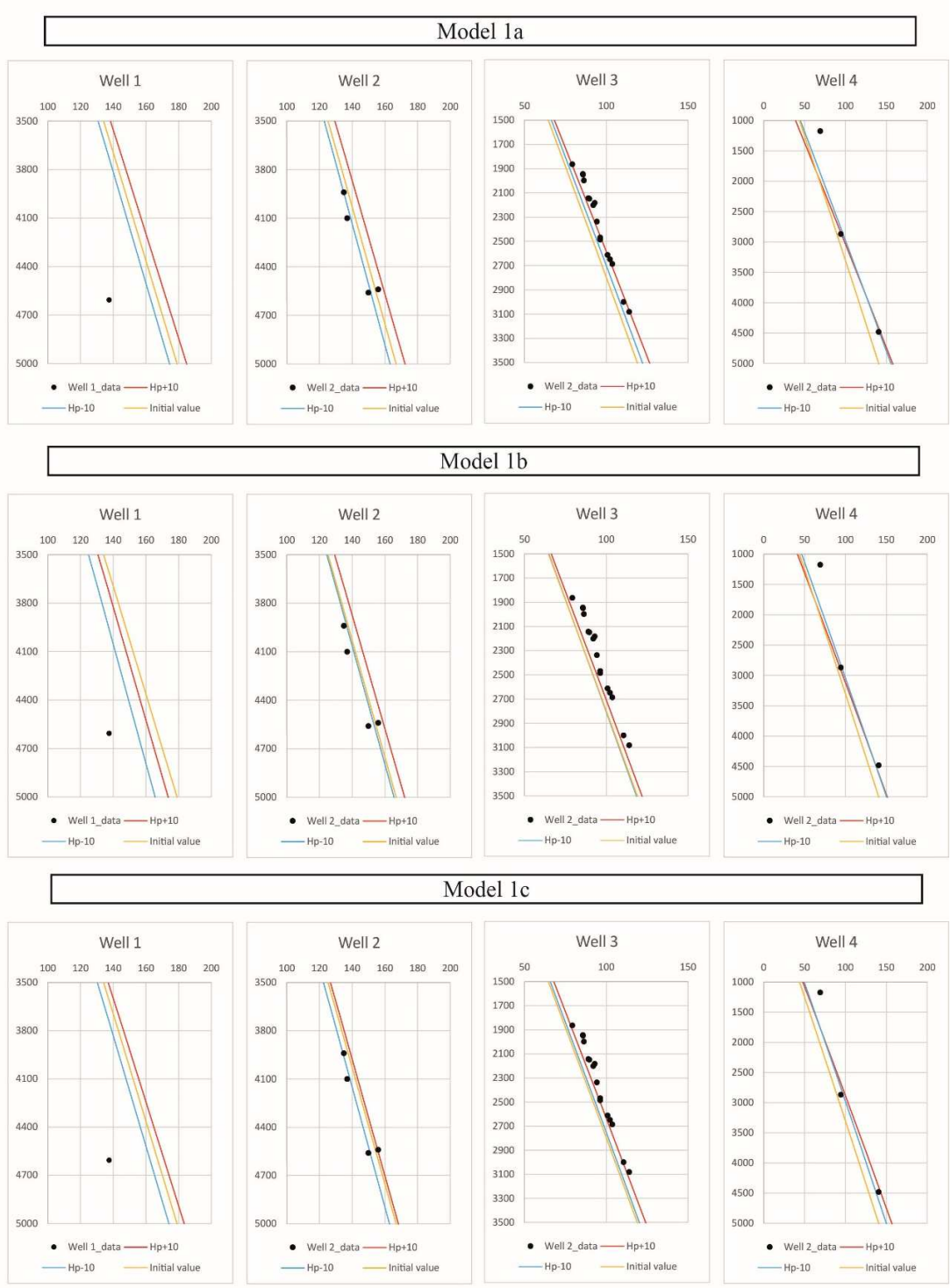

Appendix D1: We tested the sensitivity of varied radiogenic heat production on model 1a, 1b and 1c. We performed a 10% variation test for all the layers. In orange are the reference radiogenic heat production as stated in table 1. In red and blue are the sensitivity test of +10% and -10% radiogenic heat production, respectively.

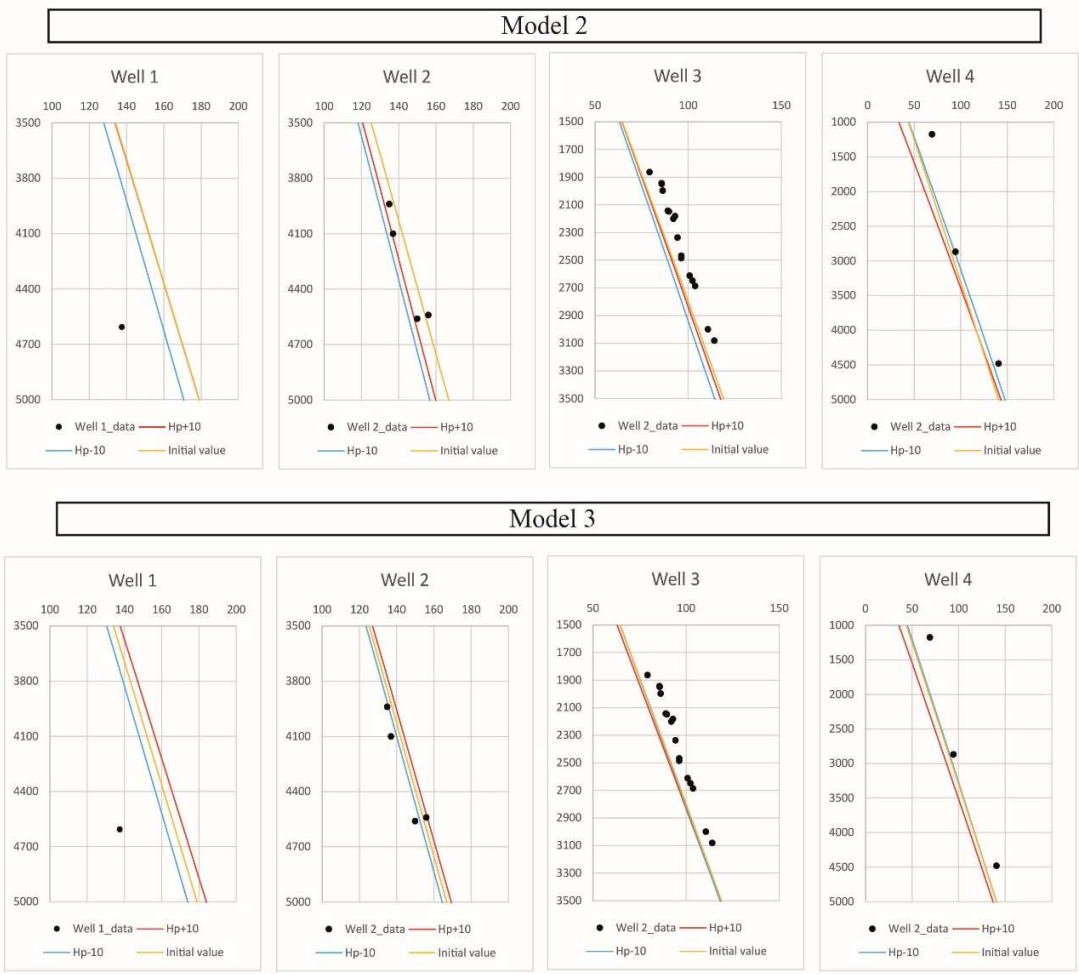

Appendix D2: We tested the sensitivity of varied radiogenic heat production on model 2 and 3. We performed a 10% variation test for all the layers together. In orange are the reference radiogenic heat production as stated in table 1. In red and blue are the sensitivity test of +10% and -10% radiogenic heat production, respectively.